

Centrifugal ultrafiltration for determination of filter cake properties of colloids

Maksym Loginov^{1,*}, Franco Samper^{1,2,3}, Geneviève Gésan-Guiziou¹, Titus Sobisch⁴,
Dietmar Lerche⁴, Eugene Vorobiev²

¹ STLO, UMR 1253, INRA, Agrocampus Ouest, 35000 Rennes, France

² UTC, TAI, Centre de Recherche de Royallieu, 60200 Compiègne, France

³ FCAI, UNCuyo, 5600 San Rafael, Mendoza, Argentina

⁴ LUM GmbH, Justus-von-Liebig-Str. 3, 12489 Berlin, Germany

*Corresponding author (maksym.loginov@gmail.com)

Highlights

Analytical centrifugal ultrafiltration is introduced

Two methods for description of centrifugal ultrafiltration kinetics are discussed

Membrane fouling, cake formation, compression and decompression are analyzed

Pressure dependency of specific cake resistance is determined via centrifugal ultrafiltration

Abstract

The article is devoted to the application of analytical centrifugation for the measurement and analysis of centrifugal ultrafiltration kinetics. The model of centrifugal ultrafiltration of colloids accounting for the cake formation, compression and possible decompression is proposed. The method for the determination of filter cake properties (pressure dependency of specific cake resistance) from the results of batch centrifugal ultrafiltration experiment is presented.

The method was tested for the determination of filterability of model samples: aqueous solutions of protein (bovine serum albumin) and nanoparticle suspension (Laponite RD). The pressure dependency of specific cake resistance was determined in the range of 10...500 kPa from the results of centrifugal ultrafiltration experiments at different centrifugal rotation speeds. The obtained values of specific resistance were in good correspondence with those measured in a series of reference constant pressure dead-end filtration tests.

Keywords: analytical centrifugation, membrane filtration, cake formation, compression-permeability, specific cake resistance.

Abbreviation

CFUF centrifugal ultrafiltration

DEF dead-end filtration

Nomenclature

a parameter of Eq. (14)

a_c centrifugal acceleration ($\text{m}\cdot\text{s}^{-2}$)

b parameter of Eq. (14)

c_0 solid concentration in the initial sample ($\text{kg}\cdot\text{m}^{-3}$)

h sample column height in centrifugal filtration cell (m)

h_0 initial sample column height in centrifugal filtration cell (m)

J filtrate flux ($\text{m}\cdot\text{s}^{-1}$)

n parameter of Eq. (11) (dimensionless)

P pressure (Pa)

P_c liquid pressure drop across filter cake (Pa)

P_m liquid pressure drop across membrane (Pa)

P_T transmembrane pressure (Pa)

p_s local solid pressure (Pa)

R distance to the membrane from the axis of rotation (m)

r_c filter cake resistance (m^{-1})

r_f fouled membrane resistance (m^{-1})

r_m membrane resistance (m^{-1})

r_T total hydraulic resistance (m^{-1})

S_m cross-sectional area of filtration membrane (m^2)

s sedimentation coefficient (s)

t time (s)

V filtrate volume (m^3)

1 w_c solid in filter cake per unit of membrane cross sectional area ($\text{kg}\cdot\text{m}^{-2}$)

2 **Greek letters**

3 α local specific cake resistance ($\text{m}\cdot\text{kg}^{-1}$)

4 $\alpha_{c,av}$ average specific cake resistance of filter cake ($\text{m}\cdot\text{kg}^{-1}$)

5 α_o parameter of Eq. (11) ($\text{m}\cdot\text{kg}^{-1}\cdot\text{Pa}^{-n}$)

6 μ liquid viscosity ($\text{Pa}\cdot\text{s}$)

7 ρ_l fluid sample (solution, suspension) specific weight ($\text{kg}\cdot\text{m}^{-3}$)

8 ρ_s specific weight of solid ($\text{kg}\cdot\text{m}^{-3}$)

9 Ω centrifugal rotation speed ($\text{rad}\cdot\text{s}^{-1}$)

10 ω material coordinate (m)

11 ω_o total solid height in filter cake (m)

12 **1. Introduction**

13 At the early stage of membrane filtration-related research (optimization of filtration
14 parameters, sample (i.e., solution, suspension) pre-treatment or membrane choice) there can be a
15 necessity of rapid characterization of filtration kinetics at different experimental conditions (e.g.,
16 transmembrane pressure), for different sample properties (pH, concentration, solvent
17 composition) and membrane type (material, molecular weight cut-off). Besides the simple
18 comparison of filtrate flux values obtained at different conditions, the research can be aimed at
19 the analysis of membrane-solute interaction (membrane fouling) and characterization of behavior
20 and properties (formation, permeability and compressibility) of the polarized layer (or filter
21 cake).

22 Currently, such a multiparametric research demands a series of separate filtration tests,
23 which is explained by technical limitations of dead-end filtration method. Several approaches
24 were proposed in order to simplify/shorten filtration experiments or replace them by the
25 measurement of a certain pertinent and accessible parameter (simple sample fluid/membrane
26 characterization):

27 (i) ones are based on empirical correlations obtained in case studies: e.g., Dahdouh et al. [1,
28 2] demonstrated a correlation between different characteristics (total soluble solids content, pH,
29 particle diameter) and filtrate flux measured in a cross-flow microfiltration of various orange

1 juice samples and suggested possible empirical prediction of filtration kinetics from the
2 determined key properties of a tested fluid; Manalo et al. [3] suggested the measurement of the
3 fluorescence intensity of biofilms formed on the surface of membrane samples after their contact
4 with studied liquid in order to predict the fouling intensity during the reverse osmosis
5 experiments.

6 (ii) others propose the characterization of filtration kinetics for a studied fluid from the
7 results of a single filtration experiment: e.g., Gesan-Guiziou et al. [4] and Espinasse et al. [5]
8 proposed different methodologies for the characterization of cross-flow filtration kinetics (critical
9 flux, fouling reversibility) by a successive variation of operational parameters (transmembrane
10 pressure, permeation flux and wall shear stress);

11 (iii) Iritani and co-authors systematically developed original methods for the complete
12 characterization of filterability (pressure dependency of specific cake resistance and cake porosity
13 in a wide pressure range) from the results of a single dead-end filtration experiment [6 – 14];

14 (iv) application of various high throughput filtration systems for the simultaneous filtration
15 of different samples at various operational conditions [15 – 20].

16 In this regard, analytical centrifugation attracts attention due to the possibility of automated
17 analysis of different samples behavior under centrifugal force [21]. Initially developed for the
18 characterization of dispersion stability and particle size analysis [22 – 24], analytical
19 centrifugation was later applied for the indirect evaluation of filterability of different samples
20 (suspensions, emulsions, protein solutions) from kinetics of centrifugal settling and consolidation
21 (papers of Iritani and co-authors [25 – 28] should be added to those briefly reviewed in [29] and
22 [30]). Recently, it was demonstrated that analytical centrifugation equipment can be used for
23 direct characterization of filterability of concentrated suspensions (pressure dependency of cake
24 dryness and specific cake resistance) via centrifugal filtration-consolidation experiments [29].
25 This gives incentive to further development of centrifugal filtration methods and theory for data
26 analysis.

27 Different theories of batch centrifugal filtration, accounting for material properties and
28 various filtration and centrifugation phenomena (particle sedimentation, pressure distribution in a
29 filter cake, pressure dependency of particle volume fraction and filtration cake resistance, filter
30 cake compression and dewatering), were developed since 1950 [31 – 49] and can be potentially
31 applied for the analysis of the results of centrifugal filtration experiment and characterization of

1 filterability. In addition, different theories of gravity filtration can be adapted for this purpose [50
2 – 57]. However, the cited methods and theories were developed for the cake filtration of
3 particulate suspensions and do not concern with the membrane fouling during the (centrifugal)
4 micro- and ultrafiltration of solutions and colloidal suspensions.

5 At the same time, centrifugal ultrafiltration is successfully applied in pharmaceutical, food
6 engineering, water treatment, nano-, bio- and chemical technology laboratories for concentration,
7 purification, clarification and washing of various colloids (proteins, DNA, nanoparticles,
8 extracts) [58 – 65]. The centrifugal filtration is usually performed with simple equipment that
9 complicates the centrifugal filtration kinetics measurement and limits the data analysis (it is
10 necessary to stop the centrifugation in order to measure the filtrate volume). To the best of the
11 author's knowledge, very limited number of papers devoted to centrifugal ultrafiltration analysis
12 is available in the literature. In this regard, systematic reports of Hideo Nakakura and co-authors
13 on centrifugal ultrafiltration must be referenced herein (e.g., [66]).

14 Recently, applications of analytical centrifugation equipment for direct characterization of
15 ultrafiltration kinetics of different samples (protein, pectin and tannin solutions) were reported
16 [67, 68]. The feasibility of semi-quantitative characterization of fluid samples filterability from
17 results of centrifugal ultrafiltration experiments was demonstrated; however, the possibility of
18 more rigorous centrifugal ultrafiltration data analysis was not discussed.

19 The present study reports the application of centrifugal ultrafiltration for characterization of
20 filterability of colloidal samples (polymer solutions, nanoparticle suspensions). The theoretical
21 part of this study was focused on the development of centrifugal ultrafiltration model accounting
22 for the peculiarities of pressure variation during the batch centrifugal filtration with cake
23 formation compression and decompression. The experimental part was devoted to the analysis of
24 centrifugal ultrafiltration curves for the quantitative characterization of membrane fouling and
25 filter cake properties: fouled membrane resistance, pressure dependency of specific cake
26 resistance and reversibility/irreversibility of cake compression.

27 **2. Model for the centrifugal ultrafiltration with cake formation**

28 **2.1. General assumptions**

29 The proposed model is based on following general assumptions.

- 30 1) The model is developed for one-dimensional batch centrifugal filtration (Fig. 1).

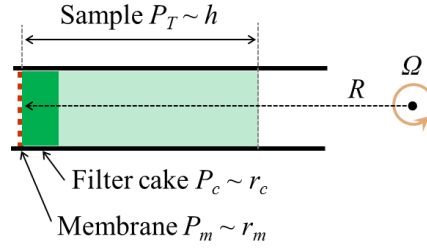


Fig. 1. Explanation for the centrifugal ultrafiltration model (P_T – transmembrane pressure, h – fluid sample height, P_c and P_m – pressure drop across the cake and the membrane, respectively, r_c and r_m – hydraulic resistance of the cake and the membrane, respectively).

2) The liquid sample (e.g., nanoparticle suspension, polymer solution) is subjected to centrifugal filtration at constant centrifugal acceleration a_c

$$a_c = \Omega^2 R \quad (1)$$

where Ω is the centrifugal rotation speed, R is the radial distance to the membrane from the axis of rotation.

3) The driving force of centrifugal filtration is the transmembrane pressure P_T , which is created by sample in filtration cell; it depends on centrifugal rotation speed Ω and the sample column height h as

$$P_T = \frac{\rho_l \Omega^2}{2} (2Rh - h^2) \quad (2)$$

where ρ_l is the sample specific weight.

4) The sample column height decreases with filtrate formation during the centrifugal filtration

$$h = h_0 - V/S_m \quad (3)$$

where h_0 is the initial sample column height, V is the filtrate volume, S_m is the cross-sectional area of filtration membrane.

5) There is complete retention of particles/polymer molecules by the membrane that results in a filter cake formation during centrifugation. If the centrifugal sedimentation rate is negligible as compared to the filtration rate (which can be a case of polymer solutions, nanoparticle suspensions), the quantity of retained solid in the filter cake per unit of membrane cross sectional area w_c can be presented as:

$$w_c = c_0 V/S_m \quad (4)$$

where c_0 is the solid concentration in the initial sample. If sedimentation cannot be neglected (as in the case of large particles or aggregates), Eq. (4) can be replaced by

$$w_c = c_0(V/S_m + sa_c t) \quad (5)$$

where s is the sedimentation coefficient and t is the centrifugal filtration time. The limitations imposed by application of Eq. (5) are discussed in Appendix A.

6) The filter cake is compressible with the pressure dependent local specific cake resistance α

$$\alpha = f(P) \quad (6)$$

Therefore, the actual hydraulic resistance of filter cake r_c can be presented as

$$r_c = \alpha_{c,av} w_c \quad (7)$$

where $\alpha_{c,av}$ denotes the average specific cake resistance, which can vary with the pressure variation during the filtration.

7) The filter cake thickness is negligible as compared to the liquid sample column height in the centrifugal filtration cell h . This is a reasonable assumption for thin filter cakes obtained during filtration of diluted colloidal samples (except of very late stages of filtration, when sample thickness tends to the filter cake thickness). Therefore, the absolute value of the liquid pressure drop across filter cake P_c can be simply presented as

$$P_c = P_T - P_m \quad (8)$$

where P_m is the liquid pressure drop across the membrane (i.e., the transmembrane pressure is distributed between the cake and the membrane). In other words, the present model neglects the influence of solid weight and liquid weight of the filter cake on the pressure distribution during the centrifugal filtration. Consequently, the filtrate flux J can be described by Darcy law as

$$J = \frac{dV}{S_m dt} = \frac{P_T}{\mu r_T} \quad (9)$$

where μ is the filtrate viscosity, r_T is the total hydraulic resistance during the filtration, which is a sum of the actual filter cake resistance r_c and constant membrane resistance r_m

$$r_T = r_m + r_c \quad (10)$$

The present model is similar to the model of dead-end filtration of colloids with significant membrane resistance proposed by Iritani et al. [10, 11]: the transmembrane pressure is redistributed between the membrane and the filter cake with constantly growing thickness. Therefore, in the frame of the present model, centrifugal ultrafiltration with compressible cake

formation is equivalent to dead-end filtration with “filtrate volume dependent” variation of applied pressure (in accordance with Eqs. (2) and (3)).

2.2. Model peculiarity: filter cakes with reversible and irreversible compression

As it follows from Eqs. (2) and (3), the important peculiarity of batch centrifugal ultrafiltration is the constant decrease of the transmembrane pressure during filtrate formation (Fig. 2).

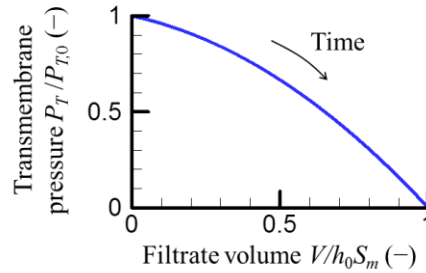


Fig. 2. Transmembrane pressure (relative to initial transmembrane pressure) versus filtrate volume (relative to initial sample volume) during the centrifugal filtration.

It was pointed out by Iritani [69] that the reversibility of filter cake compression must be taken into consideration in filtration experiments with the transmembrane pressure reduction. In the present paper two limiting cases of centrifugal ultrafiltration with filter cake formation are discussed separately: (i) filtration with completely reversible cake compression and (ii) filtration with completely irreversible cake compression.

Herein the filter cake with completely reversible cake compression is defined as a filter cake for which the actual values of local specific resistance are determined only by actual values of local solid pressure p_s . In other words, the filter cake is compressible, but elastic: its specific cake resistance is recovered after the compression-decompression cycle. According to Iritani et al. [69], this is a limiting case of completely reversible cake behavior.

The irreversibly compressible filter cake is defined as a compressible filter cake with the local properties (local specific resistance $\alpha(\omega)$) determined by the maximal value of local specific pressure $p_{s,max}(\omega)$ reached during the filtration. In other words, the structure and local specific resistance of irreversibly compressible filter cake are not recovered after any compression-

1 decompression cycle (this is the limiting case of completely irreversible cake behavior, according
2 to [69]).

3 Mathematical description and methods for simulation of centrifugal ultrafiltration with
4 completely reversible and completely irreversible cake compression are provided in Appendixes
5 A and B, respectively.

6 **2.3. Comparison with constant pressure dead-end filtration**

7 Fig. 3a presents examples of filtration curves obtained by this method for the centrifugal
8 ultrafiltration at constant centrifugal acceleration (CFUF) with formation of reversibly and
9 irreversibly compressible filter cakes. The results are compared with those calculated for the
10 dead-end filtration (DEF) with the constant transmembrane pressure equal to the initial value of
11 transmembrane pressure in the simulated CFUF experiment (Fig. 3b). For the sake of illustration,
12 it was supposed that the pressure dependency of local specific cake resistance α can be described
13 by power law equation, which is frequently used for description of colloid filter cake properties

$$\alpha = \alpha_0 p_s^n \quad (11)$$

14 where α_0 and n are parameters ($0 \leq n < 1$) and p_s is the local solid pressure (actual local solid
15 pressure for the cakes with reversible compression and maximal locally attained solid pressure
16 for the cakes with irreversible compression). It should be noted that application of Eq. (11) does
17 not lessen the generality of conclusions.

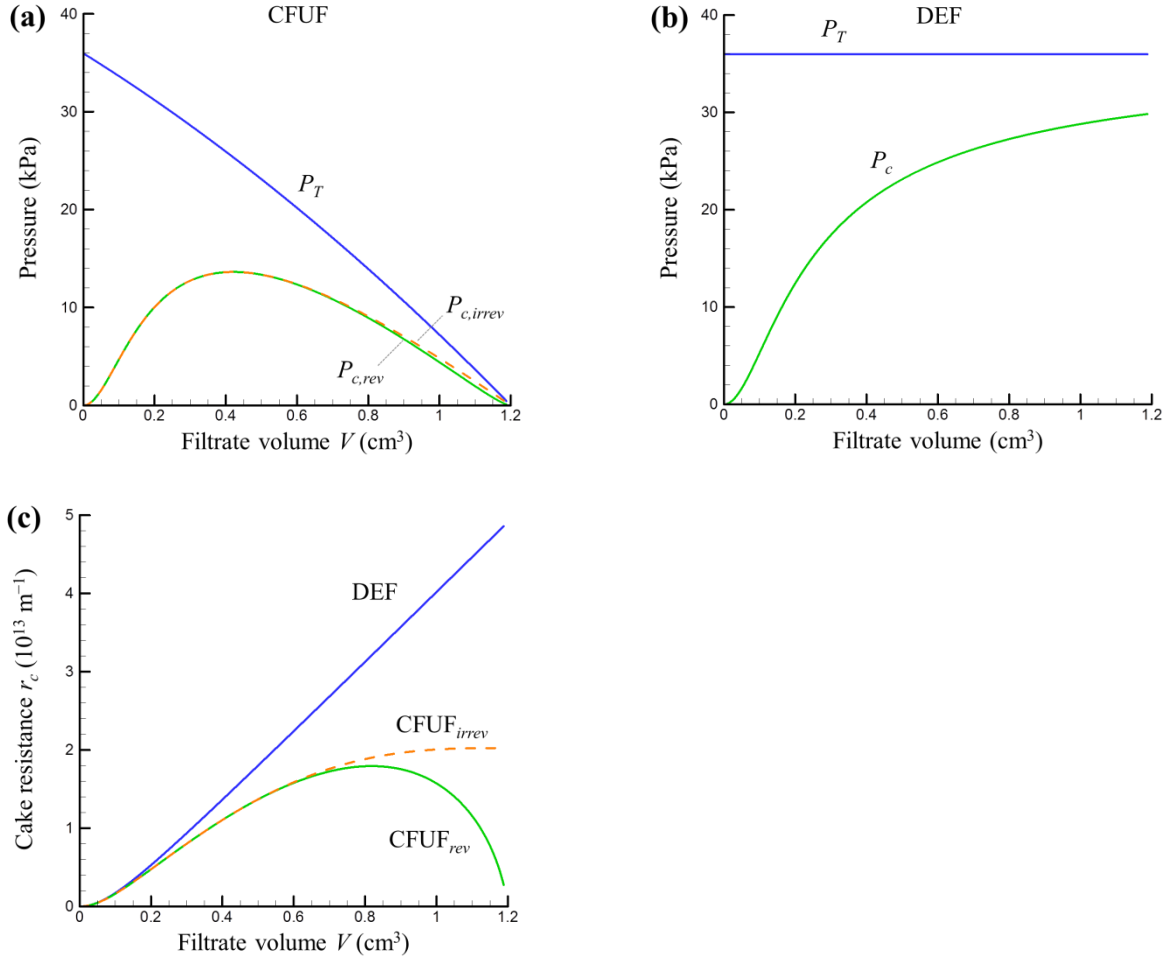


Fig. 3. Illustration for filtration with completely reversible (*rev*) and completely irreversible (*irrev*) filter cake compression: (a) transmembrane pressure P_T and liquid pressure drop across the filter cake P_c for centrifugal ultrafiltration, (b) transmembrane pressure P_T and liquid pressure drop across the filter cake P_c for constant pressure dead-end filtration, (c) cake resistance. The data simulated for centrifugal ultrafiltration at constant centrifugal acceleration (CFUF) are compared with those for the dead-end ultrafiltration at constant applied pressure (DEF). The values of parameters (which are typical for diluted colloidal samples) and operational conditions (that are representative for analytical centrifugal filtration equipment) used for the simulation are: $\Omega = 1000$ rpm, $R = 10$ cm, $r_m = 10^{13} \text{ m}^{-1}$, $n = 0.5$, $\alpha_o = 10^{13} \text{ m} \cdot \text{kg}^{-1} \cdot \text{Pa}^{-0.5}$, $h_0 = 4$ cm, $S_m = 0.3 \text{ cm}^2$, $c_0 = 1 \text{ kg} \cdot \text{m}^{-3}$, $\rho_l = 1000 \text{ kg} \cdot \text{m}^{-3}$ (the values of parameters). In CFUF the filtrate volume tends to initial sample volume $h_0 S_m = 1.2 \text{ cm}^3$.

1 In contrast to dead-end filtration, where the liquid pressure drop across the filter cake P_c
2 increases with the filter cake growth and tends towards the transmembrane pressure P_T (Fig. 3b),
3 in centrifugal filtration the value of P_c passes through a maximum (Fig. 3a). The maximum
4 position depends both on operational conditions and filter cake properties. The initial growth of
5 P_c during centrifugal filtration is explained by the transmembrane pressure redistribution between
6 cake and membrane: while the membrane resistance remains constant, the cake resistance
7 increases due to the cake growth and compression that leads to the P_c increase. The following
8 decrease of P_c originates from the gradual transmembrane pressure decrease in the centrifugal
9 filtration cell.

10 Starting from the point of maximum of P_c , centrifugal ultrafiltration with formation of
11 reversibly compressible filter cake differs from those for irreversible filter cake (Figs. 3a and 3c).
12 In experiments with reversible cake compression, the total filter cake resistance decreases with
13 the P_c decrease because of the local cake decompression (and despite of the continued cake
14 growth) (it should be noted that the maximal value of r_c is reached at higher filtrate volume as
15 compared to the maximal value of P_c , which is explained by cake growth and by compression of
16 the growing part of the cake during the P_c decrease). While in experiments with irreversibly
17 compressible cake, the filter cake resistance can only increase due to the filter cake growth after
18 the maximal P_c value is passed.

19 **3. Methods for determination of filter cake properties from centrifugal filtration** 20 **experiments**

21 Discussed peculiarities of centrifugal ultrafiltration with cake formation can be used for
22 determination of filter cake properties (i.e., filter cake compressibility, $\alpha = \alpha(p_s)$, and reversibility
23 or irreversibility of filter cake compression) from the results of centrifugal ultrafiltration
24 experiments at constant centrifugal rotation speed. Two possible methods are discussed below: (i)
25 analysis of centrifugal filtration curves (flux vs. volume) and (ii) least square fitting of
26 experimental curves to simulated centrifugal ultrafiltration curves (volume vs. time).

27 **3.1. Method of step-by-step analysis of centrifugal filtration curves**

This method does not require any supposition about filter cake properties: $\alpha(p_s)$ dependency and reversibility/irreversibility of cake compression. The method uses the following data treatment protocol:

1) the measured $V(t)$ curve is recalculated in $J(V)$, $P_T(V)$ and $w_c(V)$ (using Eqs. (9), (2) and (4), respectively);

2) the $J(V)$ and $P_T(V)$ dependencies are substituted in Eq. (2) for determination of $r_T(V)$;

3) the value of membrane resistance r_m is subtracted from $r_T(V)$ in order to obtain the $r_c(V)$ dependence;

4) the value of r_m is also used for calculation of $P_c(V)$ with the help of Darcy equation combined with Eq. (8):

$$P_c(V) = P_T(V) - \mu r_m J(V) \quad (12)$$

5) the obtained $r_c(V)$ and $w_c(V)$ are substituted in Eq. (7), and the obtained $\alpha_{c,av}(V)$ dependency is combined with $P_c(V)$ in order to obtain the $\alpha_{c,av}(P_c)$ dependency, which is then used for the analysis of cake properties (compressibility and reversibility of compression).

The method is similar to that, proposed by Iritani et al. [10, 11] for analysis of constant pressure dead-end filtration of colloids with significant membrane hydraulic resistance. However, the present method accounts for the peculiarity of the transmembrane pressure variation during the centrifugal filtration.

Fig. 4 illustrates the application of described method on example of centrifugal ultrafiltration data simulated with the help of Eq. (11).

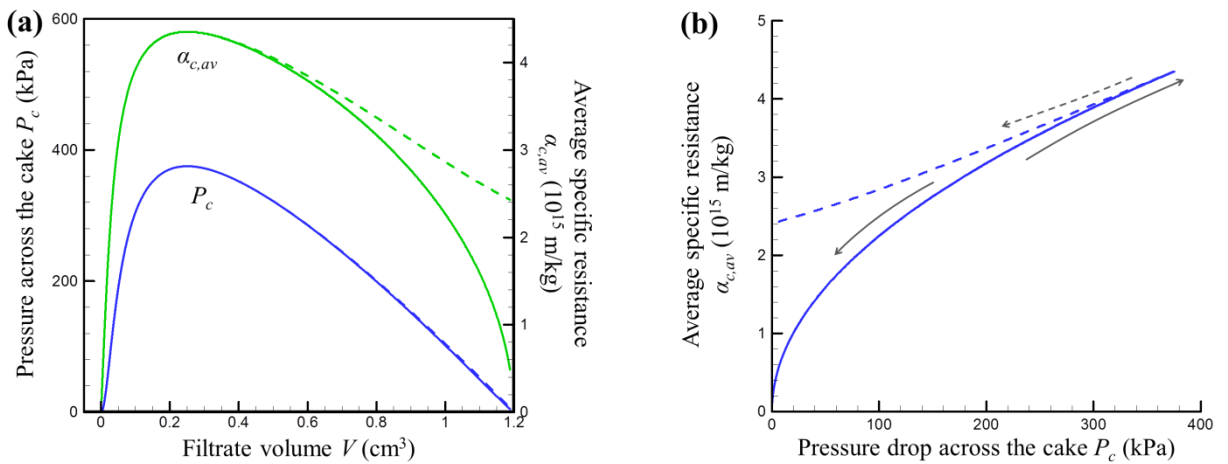


Fig. 4. Illustration for the analysis of centrifugal ultrafiltration curves (simulated data): example for completely reversible (solid curves) and irreversible (dashed curves) cake compression, (a)

Liquid pressure drop across the filter cake $P_c(V)$ and average specific cake resistance $\alpha_{c,av}(V)$ versus the filtrate volume V , (b) average specific resistance versus the liquid pressure drop $\alpha_{c,av}(P_c)$. The values of parameters and operational conditions used for the simulation are typical for diluted colloidal samples and representative for analytical centrifugal filtration equipment: $\Omega = 4000$ rpm, $R = 10$ cm, $r_m = 10^{13} \text{ m}^{-1}$, $c_0 = 1 \text{ kg} \cdot \text{m}^{-3}$, $n = 0.5$, $\alpha_o = 10^{13} \text{ m} \cdot \text{kg}^{-1} \cdot \text{Pa}^{-0.5}$, $h_0 = 4$ cm, $S_m = 0.3 \text{ cm}^2$, $\rho_l = 1000 \text{ kg} \cdot \text{m}^{-3}$. Arrows show the direction of P_c variation for reversibly and irreversibly compressible filter cake.

The increase of P_c at the first stage of filtration increases the value of $\alpha_{c,av}$ (Fig. 4a). Though the duration of this stage (i.e., time and filtrate volume required to reach the maximal value of P_c) is determined by cake properties, fluid sample quantity, membrane resistance and operational parameters, the form of obtained $\alpha_{c,av}(P_c)$ dependency is determined solely by dependency $\alpha(p_s)$, i.e., it quantitatively characterizes the sample filterability and the filter cake compressibility. As it is explained in Appendix A, the unknown $\alpha(p_s)$ dependency can be found from the obtained $\alpha_{c,av}(P_c)$ dependency with the help of the following equation

$$\alpha_{c,av}(P_c) = \frac{P_c}{\int_0^{P_c} \frac{dp_s}{\alpha}} \quad (13)$$

The range of determination of $\alpha(p_s)$ is limited by the maximal P_c value reached in the experiment (hence, it can be varied via the choice of operational parameters).

The difference in filtration behavior of the samples with reversible and irreversible cake compression at the second stage of centrifugal filtration (Fig. 4a) can be used for the evaluation of the cake compression reversibility. For reversibly compressible filter cakes, the decrease of $\alpha_{c,av}$ with the decrease of P_c at the second stage of centrifugal filtration (after the maximal value of P_c is passed) will follow the same dependency as it was obtained at the first stage of filtration (shown by solid arrows in Fig. 4b:). While for the samples with completely irreversible filter cakes compression, larger values of $\alpha_{c,av}$ will be observed for the second (descending) part of the $\alpha_{c,av}(P_c)$ dependency as compared to its first (ascending) part (Fig. 4b) (note, that the first ‘ascending’ part of the curve for irreversible cake compression fully matches that of the curve for reversibly compressible cake and can therefore not be discerned in Fig. 4b).

3.2. Method of centrifugal filtration curves fitting

As it follows from the simulation (Fig. 5), for given values of membrane resistance r_m , initial sample height h_0 and centrifugal rotation speed Ω , the dependency between filtrate volume and filtration time $V(t)$ is determined by the fluid sample and the filter cake properties (values of parameters α_o , c_0 and n).

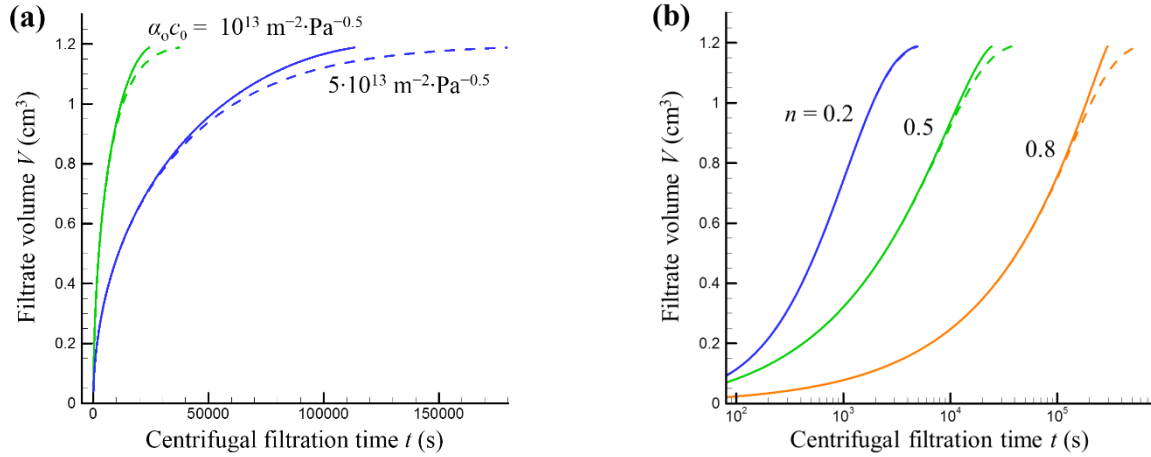


Fig. 5. Simulated curves for centrifugal ultrafiltration with completely reversible (solid curves) and completely irreversible (dashed curves) filter cake compression: (a) influence of $\alpha_o c_0$ for $n = 0.5$ and (b) influence of n for $\alpha_o c_0 = 10^{13} \text{ m}^{-2} \cdot \text{Pa}^{-n}$. Other values of parameters used for the simulation: $\Omega = 4000 \text{ rpm}$, $R = 10 \text{ cm}$, $r_m = 10^{13} \text{ m}^{-1}$, $h_0 = 4 \text{ cm}$, $S_m = 0.3 \text{ cm}^2$, $\rho_l = 1000 \text{ kg} \cdot \text{m}^{-3}$ (the values of parameters and operational conditions used for the simulation are typical for diluted colloidal samples and representative for analytical centrifugal filtration equipment).

The influence of cake properties on filtration curves is the same as for conventional dead-end filtration: the filtrate volume obtained at given time decreases with the increase of α_o , c_0 and n . In addition, the irreversible cake compression results in a lower filtrate volume at a certain time (as compared to reversible cake compression), when the point of maximal liquid pressure across the cake is passed (deviation of dashed curves from solid curves in Fig. 4). Consequently, assuming the functional dependency in Eq. (6) (for example, Eq. (11)), assuming the reversibility/ or irreversibility of the filter cake compression and fitting the simulated centrifugal ultrafiltration curves to the experimental $V(t)$ curves can yield the values of parameters determining the filter cake properties (for known values of r_m and c_0).

4. Experimental

4.1. Tested fluid samples and used membranes

Aqueous solutions with different concentrations of protein bovine serum albumin (BSA) and synthetic nanoclay Laponite were used as samples. BSA solutions with the protein weight concentration of 0.05, 0.15, 0.30, 0.45 and 0.90 % were prepared by dissolution of the lyophilized powder of BSA (purity ≥ 98 %, Sigma-Aldrich, USA) in distilled water. The obtained BSA solution had pH = 7.0. Aqueous suspension of Laponite with the weight concentration of 0.3 % was prepared by dispersion of Laponite RD (Rockwood Additives Ltd., UK) dry powder in distilled water and short sonication. The obtained Laponite suspension was transparent and had pH = 9.6.

Hydrophilic polyethersulfone ultrafiltration membranes (Microdyn-Nadir GmbH, Germany) with the nominal molecular weight cut-offs of 1 kDa and 5 kDa were used for centrifugal and constant pressure dead-end filtration experiments.

4.2. Centrifugal ultrafiltration equipment and experiments

Centrifugal ultrafiltration experiments were performed with the help of the analytical photocentrifuge Lumisizer 610 (LUM GmbH, Germany), which measures space- and time-resolved profiles of light transmission through the sample during the centrifugation [21]. Disposable plastic centrifugal filtration cells (with the filtration membrane cross sectional area of 0.35 cm^2 and the maximal sample volume of about 2 cm^3) were inserted in the centrifugal cells, used for the filtrate reception (Fig. 6). The radial position of filtration membrane from the axis of rotation R was equal to 10.2 cm. Filtration membranes were used as received (without preliminary rinsing or compaction); new membrane was used in every filtration test.

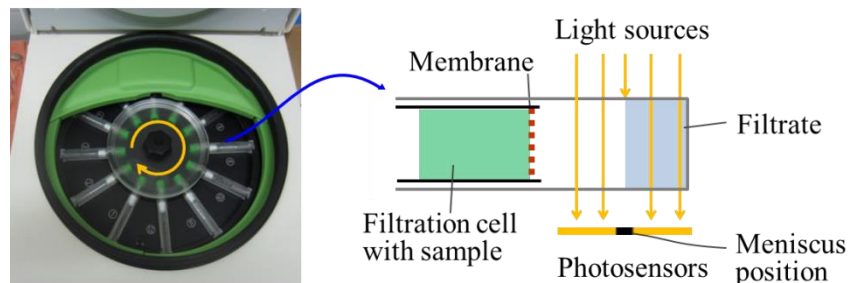


Fig. 6. Centrifugal ultrafiltration equipment and operational principle.

1 The photocentrifuge allowed simultaneous filtration of 12 different samples at centrifugal
2 rotation speed up to 4000 rpm. In the present study, the initial sample volume was constant for all
3 centrifugal experiments and equal to about 1.9 ml that corresponded to the initial sample column
4 height h_0 of 4.0 cm. Therefore, the maximal initial transmembrane pressure was equal to 570 kPa
5 (as it follows from Eq. (2)).

6 The dependency of filtrate volume on centrifugal filtration time $V(t)$ was calculated from
7 the meniscus position in centrifugal tube, which was automatically measured during the
8 centrifugation by the optical system of Lumisizer (Fig. 6) (more detail can be found elsewhere
9 [29]). Based on the nominal spatial resolution of the optical system (20 μm) and cross sectional
10 area of the centrifugal tubes used for filtrate reception in this work (0.70 cm^2), the accuracy of
11 filtrate volume measurement was estimated as $1.4 \cdot 10^{-4} \text{ cm}^3$.

12 In the present study, the experiments were carried out at constant centrifugal rotation speed
13 (1000, 2000 and 4000 rpm). The centrifugation continued until about 1.4 ml of filtrate were
14 obtained (that corresponded to the “visible by photosensors” part of the used centrifugal tubes,
15 Fig. 6). The sample temperature of 20 °C was maintained during centrifugation.

16 **4.3. Dead-end filtration experiments**

17 Constant pressure dead-end filtration was used as reference technique for sample
18 characterization. The experiments were performed with the same centrifugal filtration cells: the
19 cells were filled with studied sample and connected to the compressed air system. The constant
20 applied pressure fixed in the range of $\Delta P = 50 \dots 500 \text{ kPa}$. The filtrate volume was measured with
21 the help of an electronic balance with the accuracy of $2.2 \cdot 10^{-3} \text{ g}$. Filtration experiments were
22 performed at the room temperature of $20 \pm 1 \text{ }^\circ\text{C}$. The constant pressure dead-end filtration curves
23 were analyzed using the Ruth equation for diluted suspensions [70].

24 **4.4. Data analysis**

25 Centrifugal ultrafiltration curves were analyzed as described in sections 3.1 and 3.2. Simple
26 moving average smoothing was applied to the individual centrifugal ultrafiltration curves $V(t)$
27 before the calculation of $\alpha_{c,av}$ (section 3.1). The simulation and fitting of the simulated $V(t)$ curves
28 to the experimental data (section 3.2) was done using Maple 18 (Maplesoft, Waterloo, Canada)
29 (the corresponding script file can be obtained on simple demand from the corresponding author).

Bradford reagent was used in order to measure the protein concentration in filtrate. All of the experiments were repeated at least two times in order to confirm the tendencies (pressure dependency of the specific cake resistance). The experimental data shown in the graphs by curves and symbols represent the average values and the error bars represent standard deviation if otherwise not stated.

5. Results and discussion

5.1. Clean membrane resistance

The method of data analysis described in section 3.1 was first applied for the determination of clean membrane resistance from centrifugal ultrafiltration of distilled water (Fig. 7). The calculated value of membrane resistance remained constant despite of the transmembrane pressure variation during the experiment, and it was not dependent on the applied centrifugal rotation speed (1000...4000 rpm). It was concluded that the used membranes were not compressible (within the studied pressure range of 15...570 kPa) and had a hydraulic resistance of $(2.8 \pm 0.4) \cdot 10^{13} \text{ m}^{-1}$ (1 kDa membrane) and $(2.1 \pm 0.2) \cdot 10^{13} \text{ m}^{-1}$ (5 kDa membrane), respectively. Equal values of membrane resistance (within the experimental error range) were found from the reference experiments on continuous constant pressure dead-end filtration of distilled water.

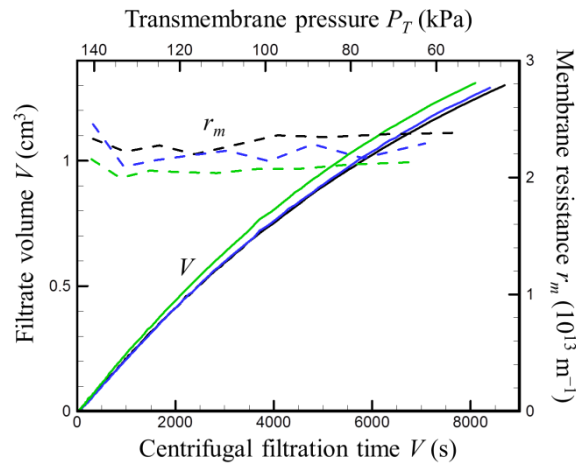


Fig. 7. Typical data on water permeation during centrifugal ultrafiltration: measured filtrate volume V (solid curves) and calculated membrane resistance r_m (dashed curves). Example for the centrifugal rotation speed of 2000 rpm. Data for three 5 kDa membrane samples tested in one

centrifuge run are presented in order to demonstrate the repeatability.

5.2. General analysis of centrifugal ultrafiltration data

Fig. 8 presents typical raw centrifugal ultrafiltration data: filtration curves obtained in the tests with different constant centrifugal rotation speeds. The general observation is the same as for the usual constant pressure dead-end filtration: filtrate volume increases with time, filtration rate continuously decreases during the filtration, and it increases with the pressure applied (caused by the increase of centrifugal rotation speed).

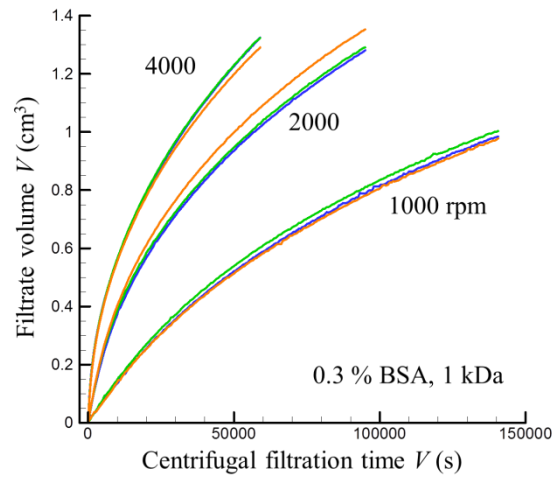


Fig. 8. Typical raw data of centrifugal ultrafiltration: dependency of filtrate volume on centrifugation time measured in tests with different constant centrifugal rotation speeds. Example for 0.3 % BSA solution tested with 1 kDa membrane at the centrifugal rotation speed of 1000, 2000 and 4000 rpm. Data for three samples tested in one centrifuge run are presented in order to demonstrate the repeatability.

The analysis of these curves is expanded in Fig. 9. As it is follows from Fig. 9a, the total resistance increased with the filtrate volume (at any studied centrifugal rotation speed). This can be attributed to membrane fouling and/or filter cake formation. It is important to note that for all studied centrifugal rotation speeds (Fig. 9a) and BSA concentrations (0.05...0.9 %, Fig. 11b) the initial total resistance, determined by graphical extrapolation of $r_T(V)$ dependency to ordinate, was significantly higher than the clean membrane resistance (which is presented in Figs. 9a and 11b by dashed line): $r_T(V = 0) \approx 8 \cdot 10^{13} \text{ m}^{-1}$ while $r_m = 2.8 \cdot 10^{13} \text{ m}^{-1}$ (for the experiments with

BSA and 1 kDa membrane). Such an abrupt (and practically independent on the transmembrane pressure) increase of membrane resistance on the beginning of ultrafiltration can be attributed to some type of membrane fouling by small quantity of solute (in the studied case of 0.3 % BSA solution it was $w_c < 1.5 \cdot 10^{-3} \text{ kg/m}^2$, corresponding to the filtrate volume $V < 0.025 \text{ cm}^3$) (it should be noted that no BSA were detected in the filtrate after the analysis with Bradford reagent). The following gradual increase of the total resistance can be attributed to the filter cake growth on the surface of the fouled membrane. Consequently, the value of fouled membrane resistance $r_f \approx 8 \cdot 10^{13} \text{ m}^{-1}$ was used instead of r_m in the following calculations of r_c , P_c and $\alpha_{c,av}$ (while the quantity of sample spent for the fouling was negligible as compared to the total quantity of filtered fluid sample and was not accounted in the present analysis). It can be noted that initial membrane fouling was significantly less pronounced during the filtration of Laponite suspensions.

The obtained $r_T(V)$ dependencies turned from concave to convex with the progress of centrifugation (Fig. 9a) in accordance with the model of cake formation (Fig. 3c). The increase of centrifugal rotation speed increased the total resistance, which can be explained by the cake compression: the calculated values of P_c increased with the centrifugal rotation speed (Fig. 9b).

The value of P_c was equal to 0 at the beginning of filtration (not seen in the logarithmic presentation in Fig. 9b) and increased proportionally to the cake resistance $P_c \sim r_c = r_T - r_f$. Therefore, the relative error of the determination of P_c was inversely proportional to the difference $r_T - r_f$. Consequently, the scattering of the calculated P_c values was important at the beginning of filtration, especially for the filter cake with low resistance (Fig. 9b, 1000 rpm). Nevertheless, rather low scattering of the calculated P_c and r_c values was observed beyond the initial stage of filtration.

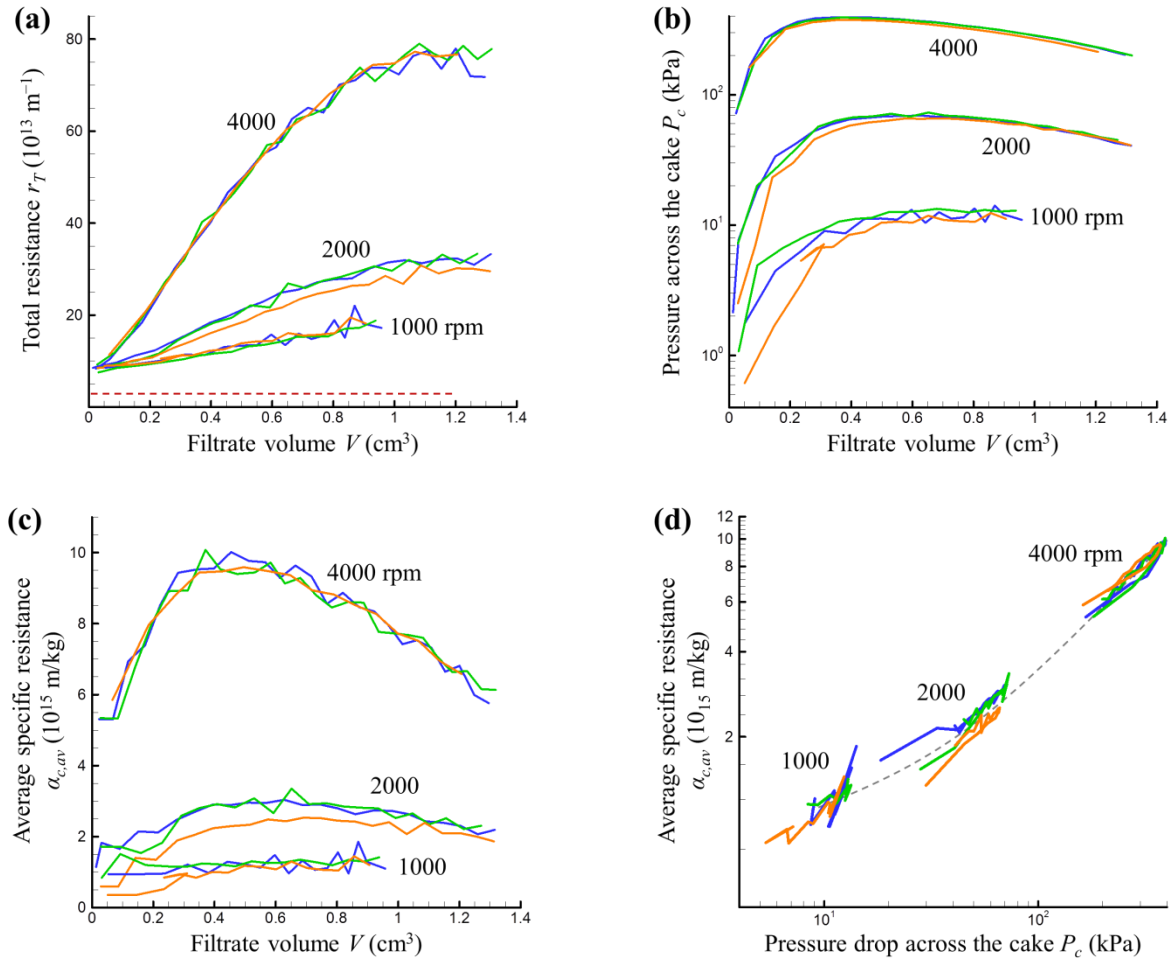


Fig. 9. Analysis of centrifugal ultrafiltration: dependency of total resistance r_T (a), pressure drop across the cake P_c (b) and average specific cake resistance $\alpha_{c,av}$ (c) on filtrate volume V , and $\alpha_{c,av}(P_c)$ dependency (d). Example for 0.3 % BSA solution tested with 1 kDa membrane at the constant centrifugal rotation speed of 1000, 2000 and 4000 rpm. Data for three samples tested in one centrifuge run are presented in order to demonstrate the repeatability. In Fig. 9a dashed line presents the clean membrane resistance. In Fig. 9d dashed line is drawn as a simple visual guide (and not a result of data fitting).

1 The calculated $P_c(V)$ dependencies passed through a maximum (in accordance with the
2 centrifugal ultrafiltration model), and the calculated $\alpha_{c,av}(V)$ dependencies passed through the
3 maximum simultaneously with $P_c(V)$ (Fig. 9c). This vindicates the supposition about the
4 compressible filter cake formation during the centrifugal ultrafiltration of BSA. The combined
5 $\alpha_{c,av}(P_c)$ dependencies are presented in Fig. 9d by polylines (the scattered points at the initial

stage of filtration are not presented). Both ascending and descending parts of the $\alpha_{c,v}(P_c)$ curves (i.e., the data obtained before and after the maximal value of P_c , respectively) are presented in Fig. 9d: in every test the difference between these parts was within the experimental error. Therefore, hypothetical irreversibility of the filter cake compression (if any) did not have any observable role in the centrifugal ultrafiltration (for the studied sample at the studied experimental conditions) and did not influence the following data analysis and conclusions (as it is shown below in Fig. 10).

In the discussed experiments, $\alpha_{c,av}(P_c)$ dependencies were determined accurately for different (non-overlapping) pressure ranges at different centrifugal rotation speeds (Fig. 9d). This suggests that characterization of $\alpha_{c,av}(P_c)$ dependency in a wide pressure range may require several tests at different centrifugal accelerations. For example, from the tests at three different centrifugal rotation speeds (1000, 2000 and 4000 rpm) it was determined for the pressure range of 7...350 kPa (in case of 0.3 % BSA sample).

5.3. Fitting of centrifugal ultrafiltration curves

The fitting of simulated centrifugal ultrafiltration curves to the raw experimental data was used as an alternative method for the determination of $\alpha_{c,av}(P_c)$ dependency. Considering the discussion above, the simulation-fitting was done simultaneously for the data obtained at different constant centrifugal rotation speeds (1000, 2000 and 4000 rpm, Fig. 10a). This is purposed to enlarge the studied pressure range and reduce the uncertainty of the determination of fitting parameters values. Raw centrifugal ultrafiltration curves were fitted using the equations, which are frequently used for characterization of colloidal samples: power law

$$\alpha_{c,av} = \alpha_0(1 - n)P_c^n \quad (14)$$

and linear

$$\alpha_{c,av} = aP_c + b \quad (15)$$

(where a and b are empirical parameters). It should be noted that Eq. (14) is obtained from the Eq. (11) under the usual assumption that Eq. (11) is applicable for the description of filter cake properties in the solid pressure range $[0...P_c]$ (from the top to the bottom of the filter cake). Therefore, Eq. (14) should be used with precautions for the sample characterization at low applied pressures (< 10 kPa in our study), when Eq. (11) can underestimate the value of specific cake resistance.

The simulation was done using the algorithm described in the Appendix B. The value of membrane resistance used for the fitting was set at $r_m = 8.0 \cdot 10^{13} \text{ m}^{-1}$. (It should be noted that in practice the value of r_m is unknown and must be also obtained by the fitting). The fitting was aimed in maximization of the sum of the determination coefficients $3r^2$, which were calculated separately for the curves obtained at three centrifugal rotation speeds. Thus the maximal possible value of the determination total determination coefficient is equal to 3 (when $r^2 = 1$ for every of three used centrifugal rotation speeds).

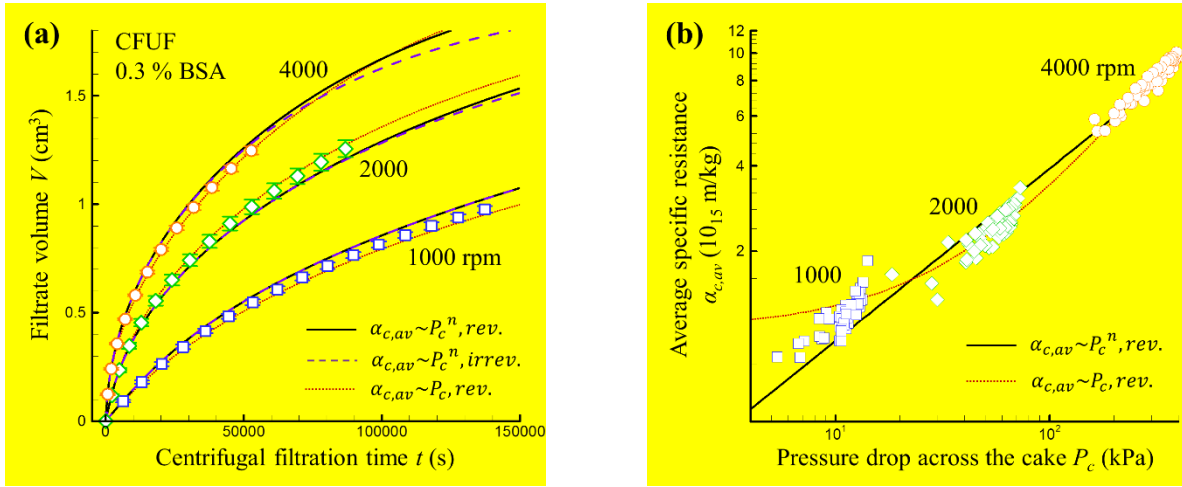


Fig. 10. (a) Experimentally measured (symbols) and simulated (curves) centrifugal ultrafiltration data: solid and dashed curves are obtained with the help of power law Eq. (14) and correspond to the reversible and irreversible filter cake compression, respectively; dotted curves are obtained with the help of linear Eq. (15) and correspond to the reversible cake compression. (b) The $\alpha_{c,av}(P_c)$ dependency determined from the step-by-step analysis of centrifugal filtration curves at different centrifugal rotation speeds (symbols) and by the simultaneous fitting of centrifugal filtration curves with the help of Eq. (14) (solid curve) and Eq. (15) (dotted curve). Example of 0.30 % BSA solutions studied at different centrifugal rotation speeds using the 1 kDa membrane.

Fig. 10a demonstrates that both power law Eq. (14) and linear Eq. (15) were appropriate for the fitting of experimental data obtained for the studied sample of 0.3 % BSA. The fitting was first done using all the measured points (both before and after the maximum of P_c) with the supposition of reversible filter cake compression. The values of best fitting parameters were: $\alpha_0 = 9.09 \cdot 10^{12} \text{ m} \cdot \text{kg}^{-1} \cdot \text{Pa}^{-n}$ and $n = 0.608$ for the total determination coefficient $3r^2 = 2.96$ (Eq. (14)) and $a = 2.38 \cdot 10^{10} \text{ m} \cdot \text{kg}^{-1} \cdot \text{Pa}^{-1}$ and $b = 1.04 \cdot 10^{15} \text{ m} \cdot \text{kg}^{-1}$ with $3r^2 = 2.98$ (Eq. (15)). Fig. 10b

demonstrates that the obtained functional dependencies (solid curve and dotted curve) were in a good correspondence with the results of the step-by-step analysis described in the previous paragraph (symbols).

The listed values of best fitting parameters of Eq. (14) were also used for the simulation of centrifugal ultrafiltration curves with the supposition of irreversible cake compression (Fig. 10a, dashed curves). The simulation demonstrated that in the studied range of filtrate volume there was no significant difference in the centrifugal ultrafiltration with reversible and irreversible filter cake compression. According to Fig. 10a, longer centrifugal ultrafiltration tests (corresponding to larger volume of filtrate and more important reduction of P_c after the maximum) are required in order to elucidate the reversibility of the filter cake compression for the studied sample. In addition, this suggests that “descending” parts of the centrifugal ultrafiltration curves can also be used in practice for the determination of the $\alpha_{c,av}(P_c)$ dependency of colloidal samples.

5.4. Impact of studied fluid sample filterability

Fig. 11 demonstrates the influence of sample filterability on centrifugal ultrafiltration behavior on example of samples with different BSA concentrations. As expected (and usually observed in conventional constant pressure dead-end filtration tests), the decrease of sample filterability (increase of the solution concentration) results in the slower centrifugal ultrafiltration. We can note that a simple comparison of raw centrifugal ultrafiltration curves (obtained for different samples at a constant centrifugal rotation speed) can be a method for the ranking of samples according to their filterability.

The specificity of batch centrifugal ultrafiltration (in comparison to conventional dead-end filtration) shows up in Figs. 11b and 11c. For the samples with low (0.05 % BSA) and high (0.9 % BSA) solute concentrations (resulting in high and low filterability, respectively), different values of total resistance can be attained during the centrifugal filtration of a limited sample volume (Fig. 11b). This results in the difference of the P_c range covered in a test with a fixed centrifugal rotation speed (i.e., lower values of P_c is attained for sample with a high filterability and vice versa). In addition, determination of the pressure dependency of $\alpha_{c,av}$ from a single centrifugal ultrafiltration test is complicated for the samples with too high filterability (e.g., 0.05 % BSA, Fig. 11d), because of the high uncertainty of the determination of r_c (which is low as compared to r_f , Fig. 11b). Nevertheless, the value of $\alpha_{c,av}$ can be approximately evaluated from

- 1 the point of maximum of P_c : for example, for the sample with 0.05 % BSA $\alpha_{c,av} = (1.7 \pm 0.2) \cdot 10^{16}$
- 2 m/kg for $P_c = 20$ kPa.

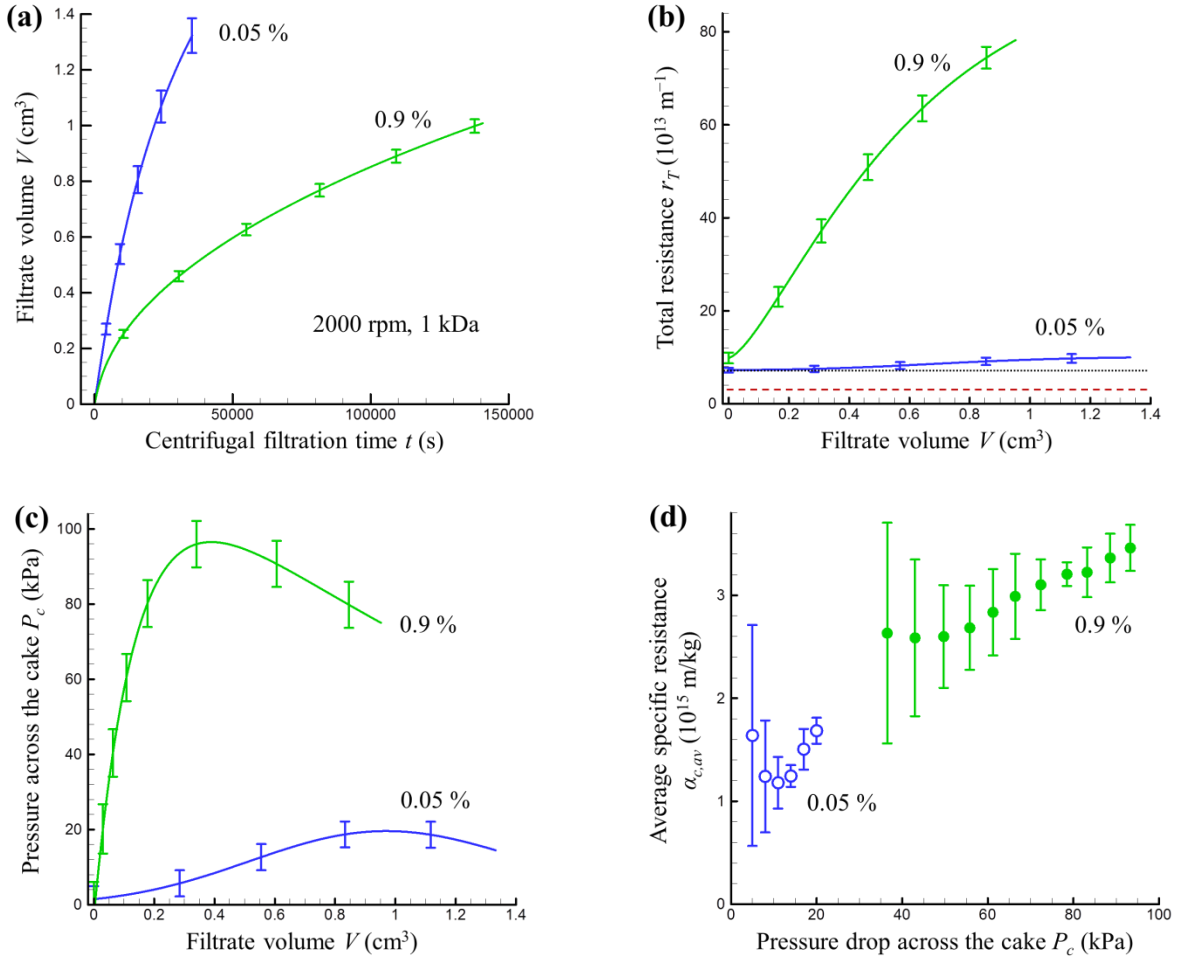


Fig. 11. Centrifugal ultrafiltration data for samples with different filterability (0.05 % and 0.9 % BSA solutions) tested with 1 kDa membrane. Example for constant centrifugal rotation speed of 2000 rpm: (a) filtrate volume $V(t)$, (b) total resistance $r_T(V)$, (c) pressure drop across the cake $P_c(V)$, (d) and average specific cake resistance $\alpha_{c,av}(P_c)$. Error bars represent standard deviations for one triplicate test. In Fig. 11b dashed and dotted lines represent r_m and r_f , respectively.

- 3 Realization of centrifugal ultrafiltration tests at different centrifugal rotation speeds allowed
- 4 to determine the $\alpha_{c,av}(P_c)$ dependencies for samples with different filterability in a wide pressure
- 5 range (Fig.12). Consistent dependences were obtained for the different BSA concentration: the
- 6 calculated values of $\alpha_{c,av}(P_c)$ were practically independent on the sample concentration (except of
- 7 the most diluted sample with 0.05 % BSA that, according to the analysis, yielded the higher

1 values of $\alpha_{c,av}$ at $P_c > 100$ kPa, as compared to more concentrated samples). In addition, the data
 2 presented in Fig. 12 confirms that the $\alpha_{c,av}(P_c)$ dependency for BSA deviates from the strong
 3 “power law type dependency” during the pressure decrease below 10 kPa and approaches a near
 4 pressure independent value of 10^{15} m/kg. The same conclusion was obtained by Iritani et al. [9,
 5 12, 13, 71] from the analysis of dead-end filtration of BSA solutions at different applied
 6 pressures.

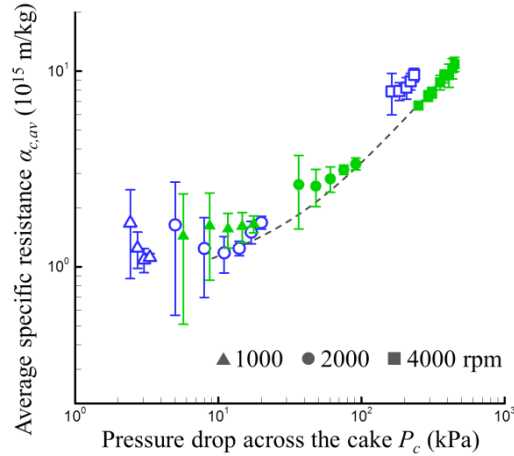


Fig. 12. Results of centrifugal ultrafiltration tests at different centrifugal rotation speeds: data for 0.05 % (open symbols) and 0.9 % (filled symbols) BSA solutions. Error bars represent standard deviations for triplicates at 1000, 2000 and 4000 (rpm). The dashed curve is the same as in Fig. 9d (i.e., represents data for 0.3 % BSA) (it is drawn as a simple visual guide).

5.4. Comparison of centrifugal and constant pressure dead-end filtration data

Fig. 13 compares the $\alpha_{c,av}(P_c)$ dependencies obtained for different samples with the help of centrifugal ultrafiltration methods proposed in this paper and conventional constant pressure dead-end filtration experiments. For the sake of better visualization the $\alpha_{c,av}(P_c)$ dependencies obtained from the analysis of centrifugal ultrafiltration curves at different centrifugal rotation speeds (1000, 2000 and 4000 rpm) are represented in Fig. 13 by the corresponding maximum points $\alpha_{c,av}(P_{c,max})$ (solid symbols).

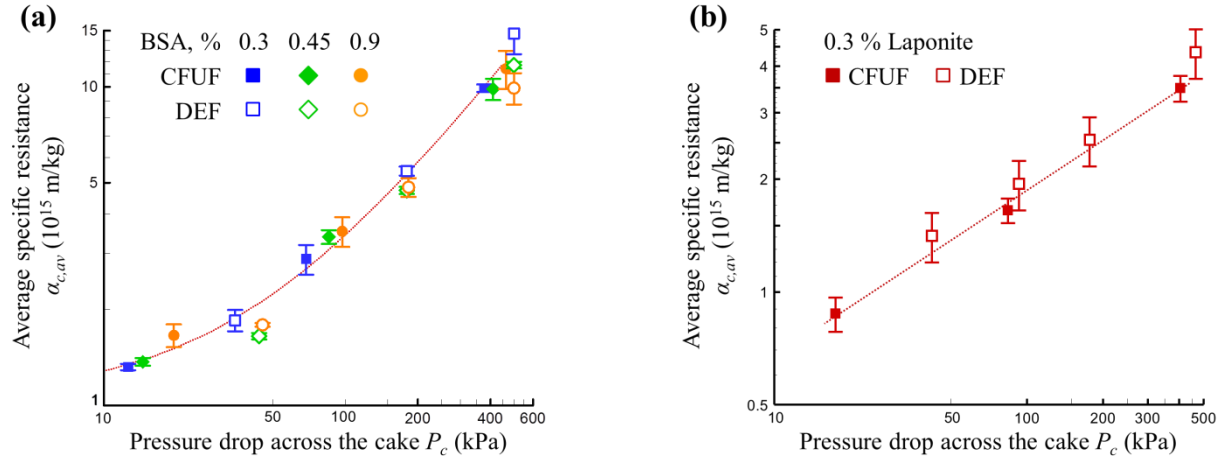


Fig. 13. Pressure dependency of average specific cake resistance $\alpha_{c,av}(P_c)$ obtained by the analysis of centrifugal ultrafiltration (CFUF, filled symbols) and conventional constant pressure dead-end filtration (DEF, open symbols) for (a) BSA solutions and (b) Laponite suspension. Dotted line in Fig 13a is obtained by the fitting of CFUF data for 0.3 % BSA with the help of Eq. (15). Dotted line in Fig. 13b is obtained by the fitting of CFUF data for 0.3 % Laponite with the help of Eq. (14). CFUF and DEF of BSA solutions were done with the 1kDa and 5 kDa membranes, respectively. CFUF and DEF of Laponite suspension were done with 5 kDa membrane.

In the case of BSA, the values of $\alpha_{c,av}$, calculated from the results of CFUF experiments, were practically independent of the BSA concentration (in the concentration range of 0.3...0.9 %). Regardless the BSA concentration, the results of CFUF analysis can be well described with the help of Eq. (15) (in the pressure range 10...500 kPa). The values of $\alpha_{c,av}$ obtained by DEF for the same pressure range were very close to those reported by Iritani et al. [9, 12, 13, 71]. The average absolute value of residual between the measured (by DEF) and predicted (from the results of CFUF with the help of Eq. (15)) values of $\alpha_{c,av}$ was equal to 12 % (of the value of $\alpha_{c,av}$ measured in DEF experiment). It should be noted that application of two different but fully retentive membranes resulted in practically same dependencies of $\alpha_{c,av}(P_c)$ obtained in CFUF (with 1 kDa membrane) and DEF (with 5 kDa membrane) experiments.

In the case of Laponite, the CFUF data were well fitted by power law Eq. (14) with the following values of parameters: $\alpha_o = 1.16 \cdot 10^{13} \text{ m} \cdot \text{kg}^{-1} \cdot \text{Pa}^{-n}$ and $n = 0.44$ with the total determination coefficient (for three experiments at 1000, 2000 and 4000) rpm of $3r^2 = 2.997$. The $\alpha_{c,av}$ values, determined from DEF experiments, were close to those determined from CFUF

analysis: the average absolute value of residual between the measured DEF and CFUF values was equal to 11 %.

Therefore, both for BSA solutions and for Laponite suspension the pressure dependencies of specific cake resistance, found by centrifugal ultrafiltration methods (centrifugal curves analysis and centrifugal curves fitting), were in reasonable agreement with those found from a series of constant pressure dead-end filtration tests in the studied pressure range of 10...500 kPa. This vindicates that the described methods of centrifugal ultrafiltration analysis can be used for the determination of pressure dependency of the specific cake resistance for colloidal samples. It should be emphasized that all centrifugal ultrafiltration data presented in Fig. 13a,b (for BSA and Laponite, including triplicates) can be obtained in only three experiments on analytical centrifugal ultrafiltration (using three different centrifugal rotation speeds). This suggests that centrifugal ultrafiltration can be used for the accelerated quantitative characterization of filterability of different samples.

6. Conclusions

Analytical centrifugation can be used for the measurement of centrifugal ultrafiltration kinetics for many different samples. The developed methods for centrifugal ultrafiltration data analysis can be used for quantitative characterization of filterability: the extent of membrane fouling and the pressure dependency of the specific cake resistance. The later can be accurately determined for a wide pressure range from the results of several centrifugal ultrafiltration tests at different constant centrifugal rotation speed.

Acknowledgments and notes

This work was partially supported by a grant of the German Federal Ministry of Economic Affairs and Energy in the frame of the program “Zentrales Innovationsprogramm Mittelstand”, which is gratefully acknowledged by the authors. ML acknowledges UTC as well as LUM GmbH and LUM team for the fruitful collaboration, thanks Dr. Wenxiang Zhang and Prof. Luhui Ding for kindly providing membrane samples and Michael Lefebvre and Jeremy Terrien for invaluable technical assistance.

The results discussed herein were partially presented during the FILTECH 2015 (Koln, Germany, 2015) and at 12th World Filtration Congress (Taipei, Taiwan, 2016).

Appendix A. Development of centrifugal ultrafiltration model

A1. Reversible cake compression

In the present article the filter cake with completely reversible cake compression is defined as a cake for which the actual values of local specific resistance α are determined by actual values of local solid pressure p_s (i.e., at any moment t in Eq. (6) $P = p_s(t)$). By analogy with the dead-end filtration theory, the actual value of average specific cake resistance $\alpha_{c,av}$ (for reversibly compressible filter cake) can be determined from the combination of integral and differential forms of Darcy law with the supposition of constant filtrate flow through the system [8]:

$$\alpha_{c,av} = \frac{P_c}{\int_0^{P_c} \frac{dp_s}{\alpha}} \quad (A1)$$

where P_c is the liquid pressure drop across the filter cake. For the sake of illustration, it was supposed that the pressure dependency of local specific cake resistance α can be described by power law equation

$$\alpha = \alpha_0 p_s^n \quad (A2)$$

where α_0 and n are parameters ($0 \leq n < 1$) (application of Eq. (A2) does not lessen the generality of conclusions). If Eq. (A2) is applied, Eq. (A1) can be reduced to the following

$$\alpha_{c,av} = \alpha_0 (1 - n) P_c^n \quad (A3)$$

and the actual filter cake resistance can be presented as

$$r_c = \alpha_0 (1 - n) P_c^n w_c \quad (A4)$$

where w_c is the solid quantity in filter cake per unit of cross sectional area of membrane. The equations Eqs. (2) – (4) and (8) – (10) (presenting the general model assumptions) can be used together with (A3) and (A4) for full description of centrifugal ultrafiltration with formation of reversibly compressible filter cake. Combination of Eqs. (8) – (10), (A3) and (A4) yields

$$(P_T - \mu r_m J)^{1-n} = (1 - n) \alpha_0 \mu J w_c \quad (A5)$$

where P_T is the transmembrane pressure, μ is the filtrate viscosity, r_m is the membrane resistance and J is the filtrate flux.

Solution of Eq. (A5) together with Eq. (2) (for the transmembrane pressure) and Eqs. (3) and (4) (accounting for the material balance) yields the dependencies of filter cake resistance r_c , liquid pressure across the cake P_c and filtrate flux J on filtrate volume V for a given combination of operational parameters (membrane resistance r_m , initial sample height h_0 and concentration c_0 ,

and constant centrifugal rotation speed Ω) and supposed parameters of constitutive equation α_0 and n (if Eq. (A2) is chosen for the filter cake description). The filtration time t can be then determined by the integration of obtained $J(V)$ dependency (or from J_i values, if Eq. (A5) is solved numerically):

$$t = \frac{1}{S_m} \int_0^V \frac{dV}{J(V)} = \frac{1}{S_m} \sum_i \frac{\Delta V}{J_i} \quad (\text{A6})$$

Appendix B presents a flow chart that can be used for the simulation of centrifugal ultrafiltration at constant centrifugal acceleration with formation of reversibly compressible filter cake.

Simulation of centrifugal filtration curves with the help of Eq. (A5) demonstrates that the liquid pressure across the filter cake P_c (and, consequently, maximal solid pressure in the filter cake) can decrease during the centrifugation (Fig. A1).

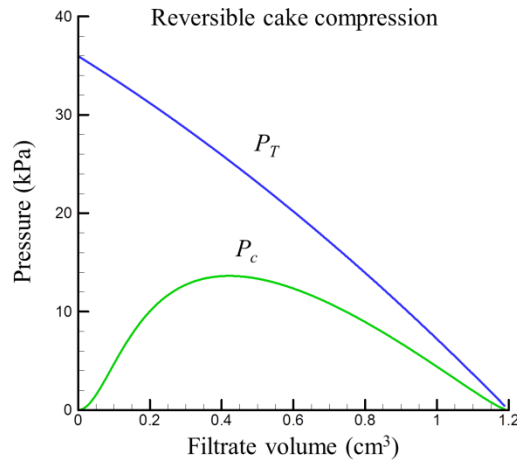


Fig. A1. Centrifugal ultrafiltration with completely reversible filter cake compression: transmembrane pressure P_T and liquid pressure drop across the filter cake P_c versus filtrate volume. Values of parameters used for the simulation with the help of Eq. (A5): $\Omega = 1000$ rpm, $R = 10$ cm, $r_m = 10^{13} \text{ m}^{-1}$, $n = 0.5$, $\alpha_0 = 10^{13} \text{ m} \cdot \text{kg}^{-1} \cdot \text{Pa}^{-0.5}$, $h_0 = 4$ cm, $S_m = 0.3 \text{ cm}^2$, $c_0 = 1 \text{ kg/m}^3$, $\rho_l = 1000 \text{ kg/m}^3$.

Below, the possibility of filter cake decompression with pressure decrease (which is the main peculiarity of centrifugal filtration with cake formation) is analyzed in details. In the centrifugal filtration with formation of reversibly compressible filter cake, the solid pressure distribution in the filter cake can be calculated in the same manner as for the dead-end filtration

[8]. Combining Eq. (A2) with the integral and differential forms of Darcy equation one can obtain [8]

$$p_s = P_c (1 - \omega/\omega_o)^{\frac{1}{1-n}} \quad (\text{A7})$$

where ω is the material coordinate (solid height in the cake) and ω_o is the total solid height in the filter cake. Since ω_o can be presented as

$$\omega_o = w_c / \rho_s \quad (\text{A8})$$

where ρ_s is the specific weight of solid, the quantity of solid in a filter cake layer with the thickness $\Delta\omega$ can be presented as

$$w = \rho_s \Delta\omega \quad (\text{A9})$$

Fig. A2a presents examples of calculated solid pressure distribution in reversibly compressible filter cake at different moments of centrifugal ultrafiltration (with the help of Eqs. (A7) and (A9) and dependence $P_c(V)$ presented in Fig. A1). The obtained $p_s(\omega)$ dependencies were recalculated in the dependencies of local specific resistance with the help of Eq. (A2) (presented in Fig. A2b as α/α_o).

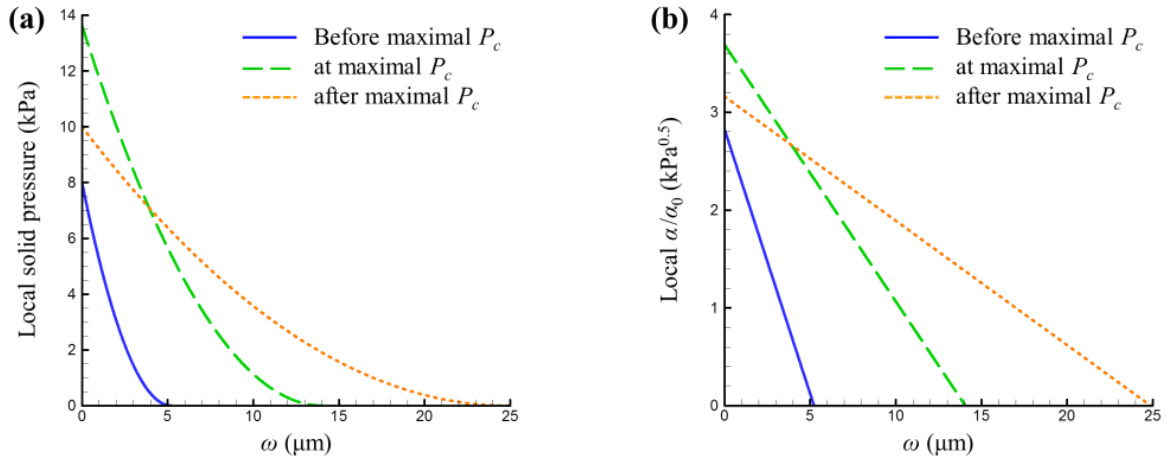


Fig. A2. Illustrative solid pressure p_s (a) and local specific cake resistance α/α_0 (b) distribution curves calculated for three moments of centrifugal ultrafiltration at constant centrifugal acceleration with formation of reversibly compressible filter cake: before the maximal value of P_c is reached (solid line), at the maximal value of P_c (dashed line) and after the maximal value of P_c is reached (dotted line). Operational parameters and sample properties are the same as in Fig. A1. The filtrate volumes V corresponding to the selected moments of filtration are equal to 0.16 ml (before maximal P_c), 0.42 ml (at maximal value of P_c) and 0.75 ml (after maximal P_c).

Until the maximal value of P_c is reached, the centrifugal filtration results in increase of local solid pressure in every point of the growing filter cake (Fig. A2a) that leads to increase of local specific cake resistance (cake compression, Fig. A2b). After the maximum of P_c is passed, the local value of solid pressure in proximity of membrane ($\omega = 0$) starts to decrease, while it continues to increase at the outer part of the filter cake (it can be demonstrated that two different $p_s(\omega)$ curves have at maximum one intersection point, if Eq. (A2) is used for description of filter cake properties). Consequently, local cake decompression (in the vicinity of membrane) and compression (in the vicinity of cake surface) happen simultaneously (Fig. A2b), if the filter cake is reversibly compressible and the filter cake properties are determined by actual values of local solid pressure (i.e., Eq. (6) is used with $P = p_s$). The partial (and progressively increasing) filter cake decompression results in filter cake resistance (r_c) decrease at late stage of centrifugal ultrafiltration (Fig. 3c).

However, different approach is required for description of irreversibly compressible filter cakes.

A2. Irreversible cake compression

Herein the irreversibly compressible filter cake is defined as a compressible filter cake with the local properties (local specific resistance $\alpha(\omega)$) determined by the maximal value of local specific pressure $p_{s,max}(\omega)$ reached during filtration (i.e., $P = p_{s,max}$ in Eq. (6)). This is the limiting case of completely irreversible cake behavior (according to Iritani et al. [69]) that can be expressed as

$$(\partial\alpha/\partial p_s)_\omega \geq 0 \text{ or } (\partial\alpha/\partial p_s)_t \geq 0 \quad (\text{A10})$$

As it follows from Figs. A1 and A2, centrifugal filtration behavior of irreversibly compressible filter cake coincides with that of reversibly compressible filter cake until the moment, when the maximal value of P_c is reached. However, the following decrease of P_c must not reduce the local values of specific resistance for irreversibly compressible filter cake (in accordance with Eq. (A10)) despite of decrease of local p_s values, which starts from the area in the vicinity of membrane surface. Consequently, a layer with constant filtration resistance starts to develop in the vicinity of membrane at the centrifugal filtration stage with decreasing P_c . This must be taken into account during the calculation of local solid pressure distribution in the entire filter cake.

The further model development proceeds from the necessity of numerical solution of centrifugal filtration equation at the stage with decreasing P_c . It is assumed that:

- 1) filtration can be discretized in steps, resulting in formation of fixed filtrate quantity ΔV at each step;
- 2) the filter cake properties, transmembrane pressure and filtrate flux remain constant during each step and vary abruptly with the passage from a previous $(i - 1)$ -th to a current i -th step;
- 3) all filter cake properties are determined for the previous, $(i - 1)$ -th, step before the passage to the next, i , step.

Eq. (A2) and corresponding derived equations are used below for the sake of illustration.

At each (for example, i -th) filtration step, irreversibly compressible filter cake can be divided into three slices (Fig. A3):

- 1) inner part 1 where the cake maintained constant local specific resistance distribution $\alpha(\omega)$ despite of local solid pressure decrease *before* the passage from $(i - 1)$ -th to i -th step;
- 2) intermediate part 2 where the local specific cake resistance distribution remained constant despite of the solid pressure decrease *with* the passage from $(i - 1)$ -th to i -th step;
- 3) outer part 3 where local specific cake resistance increased with the increase of the local solid pressure *with* the passage from $(i - 1)$ -th to i -th step.

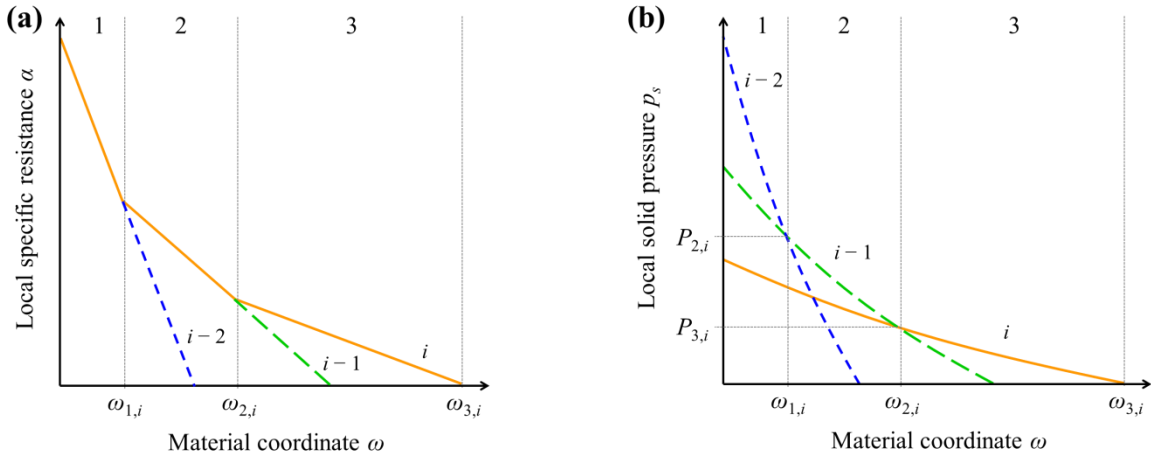


Fig. A3. Specific cake resistance distribution (a) and local solid pressure distribution (b) in the irreversibly compressible filter cake at subsequent filtration steps (the filtration stage with P_c decrease). Vertical lines separate different filter cake parts and corresponding ω ranges at step i . The dependencies $p_s(\omega)$ are illustrative and are not drawn to scale.

It can be noted that the role of part 1 in the pressure distribution is equivalent to the role of additional membrane with resistance increasing from step to step. The part defined as 2 at the i -th step of filtration is included in the part 1 at the $(i + 1)$ -th step of filtration. In addition, a certain inner region of the part 3 becomes a new part 2 at the $(i + 1)$ -th step of filtration, while outer region of the part 3 expands due to the cake growth caused by filtration: vertical lines, separating filter cake parts in Fig. A3, shift to higher ω with the passage to following filtration step.

As soon as part 3 of the cake undergoes a compression with the passage from step $i - 1$ to step i , the solid pressure distribution in this part at step i can be described with the help of rewritten Eq. (A7)

$$p_{s,i} = P_{3,i} \left(1 - \frac{\omega - \omega_{2,i}}{\omega_{3,i} - \omega_{2,i}} \right)^{\frac{1}{1-n}} \quad (\text{A11})$$

which is applicable in the range $[\omega_{2,i} \dots \omega_{3,i}]$ (Fig. A3). Here $P_{3,i}$ denotes the liquid pressure drop through the part 3 of the filter cake at step i , and the difference $\omega_{3,i} - \omega_{2,i}$ is equal to the thickness of this part (in material coordinate units).

At filtration step i , the specific cake resistance distribution in part 2 (i.e., in the range $[\omega_{1,i} \dots \omega_{2,i}]$) is determined by the local solid pressure distribution in this ω range at step $i - 1$ (according to definition of part 2). Since the filter cake was compressed in the range $[\omega_{1,i} \dots \omega_{2,i}]$ with the passage from step $i - 2$ to step $i - 1$ (Fig. A3b), the solid pressure distribution in this ω range at the step $i - 1$ also can be described by rewritten Eq. (A7)

$$p_{s,i-1} = P_{3,i-1} \left(1 - \frac{\omega - \omega_{1,i}}{\omega_{3,i-1} - \omega_{1,i}} \right)^{\frac{1}{1-n}} \quad (\text{A12})$$

The values of $(\omega_{3,i-1} - \omega_{1,i})$ and $P_{3,i-1}$ are equal to the thickness and the liquid pressure drop of the part of the cake that was defined as part 3 at the $i - 1$ step of filtration, respectively. It should be noted that Eq. (A12) accounts for the equality $P_{3,i-1} = P_{2,i}$.

At the step i , the border between parts 2 and 3 of the filter cake is situated at the point $\omega_{2,i}$, where the value of p_s did not change with the passage from step $i - 1$ to step i : $p_{s,i-1}(\omega_{2,i}) = p_{s,i}(\omega_{2,i})$. Moreover, according to Eq. (A11) the value of p_s at this point at the step i is equal to $P_{3,i}$. Therefore, substitution of $P_{3,i}$ in Eq. (A12) yields

$$\omega_{2,i} - \omega_{1,i} = (\omega_{3,i-1} - \omega_{1,i}) \left[1 - \left(\frac{P_{3,i}}{P_{3,i-1}} \right)^{1-n} \right] \quad (\text{A13})$$

As it is seen from Fig. A3, the left hand side of Eq. (A13) denotes the length of part 2 of the filter cake (in material coordinate units). Using Eq. (A9), Eq. (A13) can be presented in the terms of solid quantity in the filter cake

$$w_{2,i} = w_{3,i-1} \left[1 - \left(\frac{P_{3,i}}{P_{3,i-1}} \right)^{1-n} \right] \quad (\text{A14})$$

where $w_{2,i}$ is the solid quantity (per the unit of filter cake cross sectional area) in the part 2 of the cake at the step i of filtration and $w_{3,i-1}$ is the solid quantity in the part that was defined as part 3 at filtration step $i - 1$.

The hydraulic resistance of part 2 at the step i (denoted as $r_{2,i}$) can be calculated by the integration of expression $dr = \rho_s \alpha d\omega$ in the range $[\omega_{1,i} \dots \omega_{2,i}]$:

$$r_{2,i} = \rho_s \int_{\omega_{1,i}}^{\omega_{2,i}} \alpha d\omega \quad (\text{A15})$$

Consecutive substitution of Eq. (A12) in Eqs. (A2) and (A15) and change of the integration limits for $[P_{3,i-1} \dots P_{3,i}]$ yields

$$r_{2,i} = (1 - n) \alpha_0 w_{3,i-1} P_{3,i-1}^{n-1} (P_{3,i-1} - P_{3,i}) \quad (\text{A16})$$

At the step i the transmembrane pressure $P_{T,i}$ is distributed between three parts of filter cake and filtration membrane:

$$P_{T,i} = \mu J_i (r_m + r_{1,i} + r_{2,i} + r_{3,i}) \quad (\text{A17})$$

where $r_{1,i}$ is the resistance of part 1 of the filter cake at step i (which value is known at the step i) and $r_{3,i}$ is the resistance of part 3 that can be determined as

$$r_{3,i} = \mu J_i P_{3,i} \quad (\text{A18})$$

Substitution of Eq. (A18) in Eq. (A17) yields

$$P_{3,i} = P_{T,i} - \mu J_i (r_m + r_{1,i} + r_{2,i}) \quad (\text{A19})$$

The value of $r_{3,i}$ can be also determined with the help of Eqs. (A3) and (A4)


$$r_{3,i} = \alpha_0 (1 - n) P_{3,i}^n w_{3,i} \quad (\text{A20})$$

where $w_{3,i}$ is the quantity of solid in the part 3 of the cake at the step i . The value of $w_{3,i}$ can be obtained from the material balance in the filter cake:

$$w_{3,i} = w_{c,i} - w_{2,i} - w_{1,i} \quad (\text{A21})$$

where $w_{1,i}$ is the quantity of solid in part 1 of the filter cake at step i (which value is known at the step i). Substitution of Eq. (A21) in Eq. (A20) and combination with Eq. (A18) yields

$$J_i = \frac{P_{3,i}^{1-n}}{\mu\alpha_o(1-n)(w_{c,i} - w_{2,i} - w_{1,i})} \quad (\text{A22})$$

The system of Eqs. (A14), (A16), (A19) and (A22) can be solved at every filtration step i in order to obtain the values of four unknowns: J_i , $r_{2,i}$, $P_{3,i}$ and $w_{2,i}$. Filtration time can be later calculated with the help of Eq. (A6). Example of solution is presented in Fig. 3  (in the article).

The flow chart, which can be used for simulation of centrifugal ultrafiltration at constant centrifugal acceleration with formation of irreversibly compressible filter cake, is presented in Appendix B.

A3. Role of possible sedimentation

If necessary, the influence of sedimentation on the filter cake formation can be accounted with the help of Eq. (5). Application of Eq. (5) is required if the settling rate is comparable with filtrate flux

$$J \sim a_c s \quad (\text{A23})$$

which can be the case at the late stages of centrifugal filtration. Eq. (5) implies that the particles in the sample are monodisperse (unique value of s), and it is applicable until the following inequality is valid

$$h \geq a_c s t \quad (\text{A24})$$

At longer centrifugation time t the process is equal to the pure supernatant filtration through the formed cake.

Appendix B. Flow charts for simulation of centrifugal ultrafiltration at constant centrifugal acceleration with filter cake formation.

B1. Reversibly compressible filter cake

The following flow chart can be used for simulation of centrifugal ultrafiltration at constant centrifugal acceleration. It can be unconditionally applied for filtration with formation of reversibly compressible filter cake. In addition, it can be applied for simulation of initial part (before the maximal value of P_c is reached) of filtration with irreversible filter cake compression. It should be noted that value of ΔV does not influence dependencies on filtrate volume, but does

- 1 influence precision of determination of time dependencies. For sake of illustration, it was
- 2 supposed that filter cake compression is described by Eq. (11).

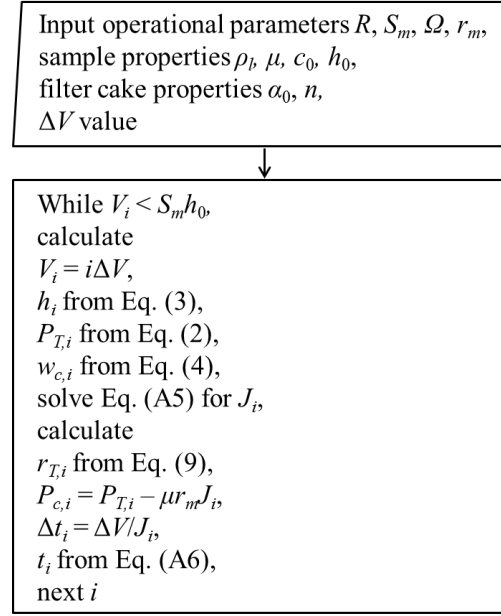


Fig. B1. Flow chart for reversibly compressible filter cakes.

3 **B2. Irreversibly compressible filter cake**

- 4 Before the maximal value of P_c is reached, centrifugal filtration curve for the irreversibly
- 5 compressible filter cake can be calculated in the same manner as for the reversibly compressible
- 6 filter cake (Appendix B1). Therefore, the flow chart for the simulation of centrifugal filtration at
- 7 constant centrifugal acceleration with formation of irreversibly compressible cake, presented in
- 8 Fig. B2, is started with the flow chart presented in Fig. B1, which is used until maximal value of
- 9 P_c is reached. It should be noted that in the flow chart presented in Fig. B2 the choice of ΔV
- 10 influences both volume and time dependencies. For sake of illustration, it was supposed that filter
- 11 cake compression is described by Eq. (11).

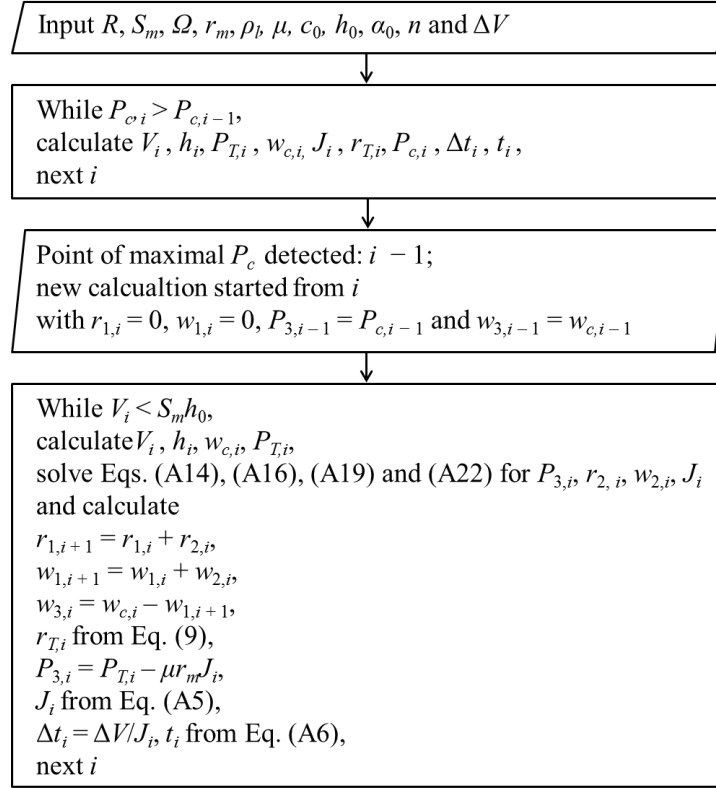


Fig. B2. Flow chart for irreversibly compressible filter cakes.

(ATTENTION, in this flow chart line J_i from Eq. (A5) is not needed)

1 **References**

- 2 [1] D. Layal, W. Christelle, R. Julien, K.-G. Andre, D. Manuel, D. Michele. Development of an
- 3 original lab-scale filtration strategy for the prediction of microfiltration performance: Application
- 4 to orange juice clarification. Separation and Purification Technology, 156 (2015) 42-50.
- 5 [2] L. Dahdouh, C. Wisniewski, A. Kapitan-Gnimdu, A. Servent, M. Dornier, M. Delalonde.
- 6 Identification of relevant physicochemical characteristics for predicting fruit juices filterability.
- 7 Separation and Purification Technology, 141 (2015) 59-67.
- 8 [3] C. V. Manalo, M. Ohno, T. Okuda, S. Nakai, W. Nishijima. Rapid novel test for the
- 9 determination of biofouling potential on reverse osmosis membranes. Water Science and
- 10 Technology, 73 (2016) 2978-2985.
- 11 [4] G. Gesan-Guiziu, E. Boyaval, G. Daufin. Critical stability conditions in crossflow
- 12 microfiltration of skimmed milk: Transition to irreversible deposition. Journal of Membrane
- 13 Science, 158 (1999) 211-222.

- [5] B. Espinasse, P. Bacchin, P. Aimar. On an experimental method to measure critical flux in ultrafiltration. *Desalination*, 146 (2002) 91-96.
- [6] T. Murase, E. Iritani, J.H. Cho, M. Shirato. Determination of filtration characteristics based upon filtration tests under step-up pressure conditions. *Journal of Chemical Engineering of Japan*, 22 (1989) 373-378.
- [7] Y. Mukai, E. Iritani, T. Murase. Effect of protein charge on cake properties in dead-end ultrafiltration of protein solutions. *Journal of Membrane Science*, 137 (1997) 271-275.
- [8] E. Iritani. Properties of filter cake in cake filtration and membrane filtration. *KONA Powder and Particle Journal*, 21 (2003) 19-39.
- [9] E. Iritani, N. Katagiri, Y. Takaishi, S. Kanetake. Determination of pressure dependence of permeability characteristics from single constant pressure filtration test. *Journal of Chemical Engineering of Japan*, 44 (2011) 14-23.
- [10] E. Iritani, N. Katagiri, Y. Sugiyama, K. Yagishita. Analysis of flux decline behaviors in filtration of very dilute suspensions. *AIChE Journal*, 53 (2007) 2275-2283.
- [11] E. Iritani, N. Katagiri, S. Kanetake. Determination of cake filtration characteristics of dilute suspension of bentonite from various filtration tests. *Separation and Purification Technology*, 92 (2012) 143-151.
- [12] E. Iritani, N. Katagiri, R. Nakajima, K.-J. Hwang, T.-W. Cheng. Cake properties of nanocolloid evaluated by variable pressure filtration associated with reduction in cake surface area. *AIChE Journal*, 60 (2014) 3869-3877.
- [13] E. Iritani, N. Katagiri, M. Tsukamoto, K.-J. Hwang. Determination of cake properties in ultrafiltration of nano-colloids based on single step-up pressure filtration test. *AIChE Journal*, 60 (2014) 289-299.
- [14] E. Iritani, N. Katagiri, R. Nakajima, K.-J. Hwang, T.-W. Cheng. Nanocolloid cake properties determined from step-up pressure filtration with single-stage reduction in filtration area. *AIChE Journal*, 61 (2015) 4426-4436.
- [15] M. Chandler, A. Zydney. High throughput screening for membrane process development. *Journal of Membrane Science*, 237 (2004) 181-188.
- [16] P. Vandezande, L. E. M. Gevers, J. S. Paul, I. F. J. Vankelecom, P. A. Jacobs. High throughput screening for rapid development of membranes and membrane processes. *Journal of Membrane Science*, 250 (2005) 305-310.

- [17] N. B. Jackson, J. M. Liddell, G. J. Lye. An automated microscale technique for the quantitative and parallel analysis of microfiltration operations. *Journal of Membrane Science*, 276 (2006) 31-41.
- [18] Y.-J. Kim, T. Yun, S. Lee, D. Kim, J. Kim. Accelerated testing for fouling of microfiltration membranes using model foulants. *Desalination*, 343 (2014) 113-119.
- [19] L. Marbelia, M. R. Bilad, A. Piassecka, P. S. Jishna, P. V. Naik, I. F. J. Vankelecom. Study of PVDF asymmetric membranes in a high-throughput membrane bioreactor (HT-MBR): Influence of phase inversion parameters and filtration performance. *Separation and Purification Technology*, 162 (2016) 6-13.
- [20] M. Kupetz, J. Aumer, D. Harms, M. Zarnkow, B. Sacher, T. Becker. High-throughput β -glucan analyses and their relationship with beer filterability. *European Food Research and Technology*, 243 (2017) 341-351.
- [21] D. Lerche, T. Sobisch. Evaluation of particle interactions by in-situ visualization of separation behavior. *Colloids and Surfaces A: Physicochemical and Engineering Aspects*, 440 (2014) 122-130.
- [22] T. Sobisch, D. Lerche, T. Detloff, M. Beiser, A. Erk. Tracing the centrifugal separation of fine-particle slurries by analytical centrifugation: Effect of centrifugal acceleration, particle interaction and concentration. *Filtration*, 6 (2006) 313 – 321.
- [23] D. Lerche, T. Sobisch. Direct and accelerated characterization of formulation stability, *Journal of Dispersion Science and Technology*, 32 (2011) 1799 – 1811.
- [24] T. Sobisch, D. Lerche, Thickener performance traced by multisample analytical centrifugation. *Colloids and Surfaces A: Physicochemical and Engineering Aspects*, 331 (2008) 114 – 118. *Colloids and Surfaces A: Physicochemical and Engineering Aspects*, 440 (2014) 122-130.
- [25] E. Iritani, K. Hattori, T. Murase. Analysis of dead-end ultrafiltration based on ultracentrifugation method. *Journal of Membrane Science*, 81 (1993) 1-13.
- [26] E. Iritani, K. Hattori, S. Akatsuka, T. Murase. Sedimentation behavior of protein solutions in ultracentrifugation field. *Journal of Chemical Engineering of Japan*, 29 (1996) 352-358.
- [27] E. Iritani, K. Hattori, T. Murase. Evaluation of Dead-End Ultrafiltration Properties by Ultracentrifugation Method. *Journal of Chemical Engineering of Japan*, 27 (1994) 357-362.

- [28] E. Iritani, N. Katagiri, K. Aoki, M. Shimamoto, K.-M. Yoo. Determination of permeability characteristics from centrifugal flotation velocity of deformable oil droplets in O/W emulsions. *Separation and Purification Technology*, 58 (2007) 247-255.
- [29] M. Loginov, N. Lebovka, E. Vorobiev. Multistage centrifugation method for determination of filtration and consolidation properties of mineral and biological suspensions using the analytical photocentrifuge. *Chemical Engineering Science*, 107 (2014) 277-289.
- [30] M. Loginov, A. Zierau, D. Kavianpour, D. Lerche, E. Vorobiev, G. Gesan-Guizieu, S. Mahnic-Kalamiza, T. Sobisch. Multistep centrifugal consolidation method for characterization of filterability of aggregated concentrated suspensions. *Separation and Purification Technology*, accepted.
- [31] N. Burak, J. Anderson Storow. Hydroextraction. Part 1. The flow relationship in a basket centrifuge. *Journal of the Society of Chemical Industry*, 69 (1950) 8-13.
- [32] M. M. Haruni, J. Anderson Storow. Hydroextraction. Techniques for permeability measurement. *Industrial and Engineering Chemistry*, 44 (1952) 2751-2756.
- [33] M. Sambuichi, H. Nakakura, K. Osasa, F. M. Tiller. Theory of batchwise centrifugal filtration. *AIChE Journal*, 33 (1987) 109-120.
- [34] M. Sambuichi, H. Nakakura, K. Osasa. Comparison of batchwise centrifugal and constant-pressure filtration. *Journal of Chemical Engineering of Japan*, 21 (1988) 418-423.
- [35] F. Fournet, J. P. Klein, G. Baluais, J. F. Remy, J. A. Dodds, D. Leclerc. Laboratory tests and methodology for the design of centrifugal filtration-washing-dewatering cycles. *Filtration and Separation*, 29 (1992) 254-260.
- [36] R. J. Wakeman. Modelling slurry dewatering and cake growth in filtering centrifuges. *Filtration and Separation*, 31 (1994) 75-81.
- [37] D. E. Smiles. Centrifugal filtration of particulate systems. *Chemical Engineering Science*, 54 (1999) 215-224.
- [38] K.-J. Hwang, W.-T. Chu, W.-M. Lu. A method to determine the cake properties in centrifugal dewatering. *Separation Science and Technology*, 36 (2001) 2693-2706.
- [39] K.-J. Hwang. Effect of particle size on the performance of batchwise centrifugal filtration. *Water Science and Technology*, 44 (2001) 185-189.

- [40] T. Friedmann, C. Lustenberger, E. J. Windhab. Filtration experiments with compressible filter cakes in centrifugal fields with superimposed static pressure. *International Journal of Mineral Processing*, 73 (2004) 261-267.
- [41] K.-J. Hwang, Y.-C. Hsieh, Y.-S. Lin. Cake formation and flux decline in centrifugal filter basket. *Journal of the Chinese Institute of Chemical Engineers*, 36 (2005) 517-525.
- [42] K.-J. Hwang, K.-H. Chou. Effect of cake compression on the performance of centrifugal dewatering. *Drying Technology*, 24 (2006) 1263-1270.
- [43] J. D. Barr, L. R. White. Centrifugal drum filtration: I. A compression rheology model of cake formation. *AIChE Journal*, 52 (2006) 545-556.
- [44] K.-J. Hwang, Y.-C. Chou. Mechanism of centrifugal filtration for separation of microbe/protein bio-suspension. *Chemical Engineering and Processing*, 47 (2008) 1647-1655.
- [45] K.-J. Hwang, Y.-C. Chou. Effects of operating conditions on the purification of protein in centrifugal filtration of bio-suspensions. *Journal of Chemical Engineering of Japan*, 41 (2008) 1102-1109.
- [46] S. H. Chan, S. Kiang, M. A. Brown. One-dimensional centrifugation model. *AIChE journal*, 49 (2009) 925-938.
- [47] A. N. Ginting, R. Fukuyama, S. M. Jami, T. Tanaka, M. Iwata. Improving slurry dewatering performance of basket centrifuge: Discharge of supernatant using bypass filter medium. *Journal of Chemical Engineering of Japan*, 48 (2015) 966-969.
- [48] R. Fukuyama, M. S. Jami, T. Tanaka, M. Iwata. Consolidation behaviour of thick suspension in centrifugal dewatering with and without supernatant. *Separation and Purification Technology*, 150 (2015) 223-228.
- [49] E. Verdurand, R. Ebert, I. Nicolaou, I. Systematical laboratory tests with a bucket centrifuge and a pressure nutsche – comparison of the cake permeability. *Chemical Engineering and Technology*, 39 (2016) 444-452.
- [50] F. M. Tiller, N. B. Hsuyng, D. Z. Cong. Role of Porosity in filtration: XII. Filtration with sedimentation. *AIChE Journal*, 41 (1995) 1153-1164.
- [51] W.-M. Lu, K.-L. Tung, C.-H. Pan. The effect of particle sedimentation on gravity filtration. *Separation Science and Technology*, 33 (1998) 1723-1746.
- [52] R. Font, P. Garcia. Permeation in sludges at low-pressure losses. *Powder Technology*, 114 (2001) 59-70.

- [53] E. Iritani, Y. Mukai, T. Yamashita. Analysis of gravity filtration behaviors of waterworks sludge based upon sedimentation tests. *Drying Technology*, 26 (2008) 1035-1043.
- [54] M. L. Christensen, D. M. Dominiak, P. H. Nielsen, K. Keiding, M. Sedin. Gravitational drainage of compressible organic materials. *AIChE Journal*, 56 (2010) 3099-3108.
- [55] D. Dominiak, M. L. Christensen, K. Keiding, P. H. Nielsen. Gravity drainage of activated sludge: New experimental method and considerations of settling velocity, specific cake resistance and cake compressibility. *Water Research*, 45 (2011) 1941-1950.
- [56] M. L. Christensen, K. Keiding. Numerical model of gravity drainage of compressible organic slurries. *Powder Technology*, 217 (2012) 189-198.
- [57] S. G. Sveegaard, K. Keiding, M. L. Christensen. Compression and swelling of activated sludge cakes during dewatering. *Water Research*, 46 (2012) 4999-5008.
- [58] R. M. Geanta, M. Olga Ruiz, I. Escudero. Micellar-enhanced ultrafiltration for the recovery of lactic acid and citric acid from beet molasses with sodium dodecyl sulphate. *Journal of Membrane Science*, 430 (2013) 11-23.
- [59] A. M. Sanchez, M. Carmona, M. Prodanov, G. L. Alonso. Effect of centrifugal ultrafiltration on the composition of aqueous extracts of saffron spice (*Crocus sativus* L.). *Journal of Agricultural and Food Chemistry*, 56 (2008) 7293-7301.
- [60] E. E. Borujeni, A. L. Zydney. Separation of plasmid DNA isoforms using centrifugal ultrafiltration. *BioTechniques*, 53 (2012) 49-56.
- [61] Y. Shen, M. Y. Gee, A. B. Greytak. Purification technologies for colloidal nanocrystals. *Chemical Communications*, 53 (2017) 827-841.
- [62] G. Dalwadi, H. A. E. Benson, Y. Chen. Comparison of diafiltration and tangential flow filtration for purification of nanoparticle suspensions. *Pharmaceutical Research*, 22 (2005) 2152-2162.
- [63] N. Alele, R. Streubel, L. Gamrad, S. Barcikowski, M. Ulbricht. Ultrafiltration membrane-based purification of bioconjugated gold nanoparticle dispersions. *Separation and Purification Technology*, 157 (2016) 120-130.
- [64] A. Eppler, M. Weigandt, S. Schulze, A. Hanefeld, H. Bunjes. Comparison of different protein concentration techniques within preformulation development. *International Journal of Pharmaceutics*, 421 (2011) 120-129.

- [65] H. Wei, X. Zhang, X. Tian, G. Wu. Pharmaceutical applications of affinity-ultrafiltration mass spectrometry: Recent advances and future prospects. *Journal of Pharmaceutical and Biomedical Analysis*, 131 (2016) 444-453.
- [66] H. Nakakura, A. Tsubone, K. Miura, K. Osasa. Centrifugal ultrafiltration of protein solutions in a centripetal-flow cell. *Proceedings of the 10th Congress of Asian Pacific Confederation of Chemical Engineering*, 2004, Kitakyushuu, Japan.
- [67] M. Loginov, N. Lebovka, E. Vorobiev. Use of photocentrifuge for membrane separation and characterization of solutions filterability. *Proceedings of the International Conference for Filtration and Separation Technology FILTECH 2015*, 2015, Koln, Germany.
- [68] M. Loginov, E. Vorobiev, T. Sobisch, D. Lerche. Accelerated analysis of filterability: ultrafiltration in the photocentrifuge. *Proceedings of the 12th World Filtration Congress*, 2016, Taipei, Taiwan.
- [69] E. Iritani, N. Katagiri, G. Inagaki. Compression and expansion properties of filter cake accompanied with step change in applied pressure in membrane filtration. *Separation and Purification Technology*, (2016) in press.
- [70] M. Loginov, K. Loginova, N. Lebovka, E. Vorobiev. Comparison of dead-end ultrafiltration behaviour and filtrate quality of sugar beet juices obtained by conventional and "cold" PEF-assisted diffusion. *Journal of Membrane Science*, 377 (2011) 273-283.
- [71] E. Iritani, Y. Mukai, E. Hagihara. Measurements and evaluation of concentration distributions in filter cake formed in dead-end ultrafiltration of protein solutions. *Chemical Engineering Science*, 57 (2002) 53-62.

Figure captions

Fig. 1. Explanation for the centrifugal ultrafiltration model (P_T – transmembrane pressure, h – fluid sample height, P_c and P_m – pressure drop across the cake and the membrane, respectively, r_c and r_m – hydraulic resistance of the cake and the membrane, respectively).

Fig. 2. Transmembrane pressure (relative to initial transmembrane pressure) versus filtrate volume (relative to initial sample volume) during the centrifugal filtration.

Fig. 3. Illustration for filtration with completely reversible (*rev*) and completely irreversible (*irrev*) filter cake compression: (a) transmembrane pressure P_T and liquid pressure drop across the filter cake P_c for centrifugal ultrafiltration, (b) transmembrane pressure P_T and liquid pressure drop across the filter cake P_c for constant pressure dead-end filtration, (c) cake resistance. The data simulated for centrifugal ultrafiltration at constant centrifugal acceleration (CFUF) are compared with those for the dead-end ultrafiltration at constant applied pressure (DEF). The values of parameters (which are typical for diluted colloidal samples) and operational conditions (that are representative for analytical centrifugal filtration equipment) used for the simulation are: $\Omega = 1000$ rpm, $R = 10$ cm, $r_m = 10^{13}$ m⁻¹, $n = 0.5$, $\alpha_o = 10^{13}$ m·kg⁻¹·Pa^{-0.5}, $h_0 = 4$ cm, $S_m = 0.3$ cm², $c_0 = 1$ kg·m⁻³, $\rho_l = 1000$ kg·m⁻³ (the values of parameters). In CFUF the filtrate volume tends to initial sample volume $h_0 S_m = 1.2$ cm³.

Fig. 4. Illustration for the analysis of centrifugal ultrafiltration curves (simulated data): example for completely reversible (solid curves) and irreversible (dashed curves) cake compression, (a) Liquid pressure drop across the filter cake $P_c(V)$ and average specific cake resistance $\alpha_{c,av}(V)$ versus the filtrate volume V , (b) average specific resistance versus the liquid pressure drop $\alpha_{c,av}(P_c)$. The values of parameters and operational conditions used for the simulation are typical for diluted colloidal samples and representative for analytical centrifugal filtration equipment: $\Omega = 4000$ rpm, $R = 10$ cm, $r_m = 10^{13}$ m⁻¹, $c_0 = 1$ kg·m⁻³, $n = 0.5$, $\alpha_o = 10^{13}$ m·kg⁻¹·Pa^{-0.5}, $h_0 = 4$ cm, $S_m = 0.3$ cm², $\rho_l = 1000$ kg·m⁻³. Arrows show the direction of P_c variation for reversibly and irreversibly compressible filter cake.

Fig. 5. Simulated curves for centrifugal ultrafiltration with completely reversible (solid curves) and completely irreversible (dashed curves) filter cake compression: (a) influence of $\alpha_o c_0$ for $n = 0.5$ and (b) influence of n for $\alpha_o c_0 = 10^{13}$ m⁻²·Pa^{- n} . Other values of parameters used for the simulation: $\Omega = 4000$ rpm, $R = 10$ cm, $r_m = 10^{13}$ m⁻¹, $h_0 = 4$ cm, $S_m = 0.3$ cm², $\rho_l = 1000$ kg·m⁻³ (the values of parameters and operational conditions used for the simulation are typical for diluted colloidal samples and representative for analytical centrifugal filtration equipment).

Fig. 6. Centrifugal ultrafiltration equipment and operational principle.

Fig. 7. Typical data on water permeation during centrifugal ultrafiltration: measured filtrate volume V (solid curves) and calculated membrane resistance r_m (dashed curves). Example for the

centrifugal rotation speed of 2000 rpm. Data for three 5 kDa membrane samples tested in one centrifuge run are presented in order to demonstrate the repeatability.

Fig. 8. Typical raw data of centrifugal ultrafiltration: dependency of filtrate volume on centrifugation time measured in tests with different constant centrifugal rotation speeds. Example for 0.3 % BSA solution tested with 1 kDa membrane at the centrifugal rotation speed of 1000, 2000 and 4000 rpm. Data for three samples tested in one centrifuge run are presented in order to demonstrate the repeatability.

Fig. 9. Analysis of centrifugal ultrafiltration: dependency of total resistance r_T (a), pressure drop across the cake P_c (b) and average specific cake resistance $\alpha_{c,av}$ (c) on filtrate volume V , and $\alpha_{c,av}(P_c)$ dependency (d). Example for 0.3 % BSA solution tested with 1 kDa membrane at the constant centrifugal rotation speed of 1000, 2000 and 4000 rpm. Data for three samples tested in one centrifuge run are presented in order to demonstrate the repeatability. In Fig. 9a dashed line presents the clean membrane resistance. In Fig. 9d dashed line is drawn as a simple visual guide (and not a result of data fitting).

Fig. 10. (a) Experimentally measured (symbols) and simulated (curves) centrifugal ultrafiltration data: solid and dashed curves are obtained with the help of power law Eq. (14) and correspond to the reversible and irreversible filter cake compression, respectively; dotted curves are obtained with the help of linear Eq. (15) and correspond to the reversible cake compression. (b) The $\alpha_{c,av}(P_c)$ dependency determined from the step-by-step analysis of centrifugal filtration curves at different centrifugal rotation speeds (symbols) and by the simultaneous fitting of centrifugal filtration curves with the help of Eq. (14) (solid curve) and Eq. (15) (dotted curve). Example of 0.30 % BSA solutions studied at different centrifugal rotation speeds using the 1 kDa membrane.

Fig. 11. Centrifugal ultrafiltration data for samples with different filterability (0.05 % and 0.9 % BSA solutions) tested with 1 kDa membrane. Example for constant centrifugal rotation speed of 2000 rpm: (a) filtrate volume $V(t)$, (b) total resistance $r_T(V)$, (c) pressure drop across the cake $P_c(V)$, (d) and average specific cake resistance $\alpha_{c,av}(P_c)$. Error bars represent standard deviations for one triplicate test. In Fig. 11b dashed and dotted lines represent r_m and r_f , respectively.

Fig. 12. Results of centrifugal ultrafiltration tests at different centrifugal rotation speeds: data for 0.05 % (open symbols) and 0.9 % (filled symbols) BSA solutions. Error bars represent standard

deviations for triplicates at 1000, 2000 and 4000 (rpm). The dashed curve is the same as in Fig. 9d (i.e., represents data for 0.3 % BSA) (it is drawn as a simple visual guide).

Fig. 13. Pressure dependency of average specific cake resistance $\alpha_{c,av}(P_c)$ obtained by the analysis of centrifugal ultrafiltration (CFUF, filled symbols) and conventional constant pressure dead-end filtration (DEF, open symbols) for (a) BSA solutions and (b) Laponite suspension. Dotted line in Fig 13a is obtained by the fitting of CFUF data for 0.3 % BSA with the help of Eq. (15). Dotted line in Fig. 13b is obtained by the fitting of CFUF data for 0.3 % Laponite with the help of Eq. (14). CFUF and DEF of BSA solutions were done with the 1kDa and 5 kDa membranes, respectively. CFUF and DEF of Laponite suspension were done with 5 kDa membrane.

Fig. A1. Centrifugal ultrafiltration with completely reversible filter cake compression: transmembrane pressure P_T and liquid pressure drop across the filter cake P_c versus filtrate volume. Values of parameters used for the simulation with the help of Eq. (A5): $\Omega = 1000$ rpm, $R = 10$ cm, $r_m = 10^{13} \text{ m}^{-1}$, $n = 0.5$, $\alpha_o = 10^{13} \text{ m} \cdot \text{kg}^{-1} \cdot \text{Pa}^{-0.5}$, $h_0 = 4$ cm, $S_m = 0.3 \text{ cm}^2$, $c_0 = 1 \text{ kg/m}^3$, $\rho_l = 1000 \text{ kg/m}^3$.

Fig. A2. Illustrative solid pressure p_s (a) and local specific cake resistance α/α_0 (b) distribution curves calculated for three moments of centrifugal ultrafiltration at constant centrifugal acceleration with formation of reversibly compressible filter cake: before the maximal value of P_c is reached (solid line), at the maximal value of P_c (dashed line) and after the maximal value of P_c is reached (dotted line). Operational parameters and sample properties are the same as in Fig. A1. The filtrate volumes V corresponding to the selected moments of filtration are equal to 0.16 ml (before maximal P_c), 0.42 ml (at maximal value of P_c) and 0.75 ml (after maximal P_c).

Fig. A3. Specific cake resistance distribution (a) and local solid pressure distribution (b) in the irreversibly compressible filter cake at subsequent filtration steps (the filtration stage with P_c decrease). Vertical lines separate different filter cake parts and corresponding ω ranges at step i . The dependencies $p_s(\omega)$ are illustrative and are not drawn to scale.

Fig. B1. Flow chart for reversibly compressible filter cakes.

Fig. B2. Flow chart for irreversibly compressible filter cakes.